DNP-Enhanced Solid-State NMR Spectroscopy of Active Pharmaceutical Ingredients

Li Zhao,[1,2] Arthur C. Pinon,[3] Lyndon Emsley[3] and Aaron J. Rossini*[1,2]

[1]*Iowa State University, Department of Chemistry, Ames, IA, USA*

[2]*US DOE Ames Laboratory, Ames, Iowa, USA*

[3]*Institut des Sciences et Ingénierie Chimiques, Ecole Polytechnique Fédérale de Lausanne (EPFL), CH-1015 Lausanne, Switzerland*

AUTHOR INFORMATION

Corresponding Author

Aaron J. Rossini, e-mail: arossini@iastate.edu

This article has been accepted for publication and undergone full peer review but has not been through the copyediting, typesetting, pagination and proofreading process which may lead to differences between this version and the Version of Record. Please cite this article as doi: 10.1002/mrc.4688

Abstract

Solid-state NMR has become a valuable tool for the characterization of both pure and formulated active pharmaceutical ingredients (APIs). However, NMR generally suffers from poor sensitivity that often restricts NMR experiments to nuclei with favorable properties, concentrated samples and acquisition of 1D NMR spectra. Here we review how dynamic nuclear polarization (DNP) can be applied to routinely enhance the sensitivity of solid-state NMR experiments by one to two orders of magnitude for both pure and formulated APIs. Sample preparation protocols for relayed DNP experiments and experiments on directly-doped APIs are detailed. Numerical spin diffusion models illustrate the dependence of relayed DNP enhancements on the relaxation properties and particle size of the solids and can be used for particle size determination when the other factors are known. We then describe the advanced solid-state NMR experiments that have been enabled by DNP and how they provide unique insight into the molecular and macroscopic structure of APIs. For example, with large sensitivity gains provided by DNP natural isotopic abundance ^{13}C-^{13}C DQ-SQ homonuclear correlation NMR spectra of pure APIs can be routinely acquired. DNP-enhanced solid-state NMR also enables solid-state NMR experiments with unreceptive quadrupolar nuclei such as ^{2}H, ^{14}N and ^{35}Cl that are commonly found in APIs. Applications of DNP-enhanced solid-state NMR for the molecular level characterization of low API load formulations such as commercial tablets and amorphous solid dispersions are described. Future perspectives for DNP-enhanced solid-state NMR experiments on APIs are briefly discussed.

Introduction

Approximately two thirds of active pharmaceutical ingredients (APIs) are administered as solid dosage forms. The solid-state structure of APIs strongly affects the stability, solubility and ultimately the efficacy of APIs within dosage forms.[1-4] Consequently, APIs are often prepared in different solid forms in order to identify the forms that are most suitable for formulation. For example, by varying recrystallization conditions it is possible to isolate polymorphs of APIs that possess unique crystal structures and offer different stabilities and solubility.[5-9] APIs are often reacted with crystal coformers to obtain multicomponent solids (i.e., cocrystals or salts) that display enhanced solubility and/or stability.[10-15] Alternatively, some APIs are deployed as amorphous forms in order to enhance dissolution rates and solubility.[16-19] However, amorphous APIs must be stabilized to prevent crystallization and this is usually accomplished by mixing the amorphous API with polymers to form amorphous solid dispersions (ASDs).[16-20] These examples demonstrate that the development and deployment of APIs in formulations requires identification and characterization of the different possible solid forms of a particular API. Typically the solid-state structure of APIs or multicomponent solids are determined with single crystal X-ray diffraction, however, for many solids it is challenging to isolate diffraction quality single crystals and in the case of amorphous APIs diffraction methods will likely not be applicable. Characterization of formulated APIs (i.e., tablets) is especially challenging because interference from the highly abundant excipients and the low concentration of the API hinders diffraction and other analytical techniques.

Solid-state NMR spectroscopy is now an established method for the characterization of pure, multicomponent (i.e., cocrystals and ASDs) and formulated APIs. Many excellent reviews and books describe the established applications of solid-state NMR spectroscopy to APIs.[21-37] One key application of solid-state NMR spectroscopy to APIs is the identification and differentiation of polymorphs. Early in the development of high-resolution solid-state NMR it was shown that ^{13}C solid-state NMR spectroscopy could differentiate polymorphs of APIs on the basis of slight differences in the observed isotropic ^{13}C chemical shifts.[26,32,38-43] Consequently, ^{13}C solid-state NMR has been widely applied for identification (“fingerprinting”) and quantification of polymorphs of APIs in mixtures and/or dosage forms. Measurements of ^{1}H longitudinal relaxation times (T_1) and/or rotating frame longitudinal relaxation times ($T_{1\rho}$) are often used to obtain information about the domain/grain size of the APIs and determine the proximity of the API to excipients/coformers/stabilizers.[30,44,45] Advances in NMR technology and methods have also improved the analysis of APIs by solid-state NMR spectroscopy. For example, fast magic angle spinning (MAS)[46-50] and/or homonuclear ^{1}H decoupling (i.e., CRAMPS)[51] are now routinely employed to obtain high-resolution ^{1}H solid-state NMR spectra of APIs and organic solids.[46,50,52,53] Solid-state ^{1}H chemical shifts are

distinct for different polymorphic forms of APIs[53-60] and ^{1}H solid-state NMR offers much higher sensitivity than ^{13}C solid-state NMR.

In favorable cases, crystal structures may be experimentally determined with solid-state NMR spectroscopy, possibly in conjunction with quantum chemical calculations. For example, ^{1}H-^{1}H distances measured by solid-state NMR were used to determine the crystal structure of β-L-aspartyl-L-alanine.[52,61] ^{1}H-^{1}H, ^{1}H-^{13}C and ^{13}C-^{13}C internuclear distances were used to determine the molecular structure of ^{13}C labeled L-tyrosine ethyl ester in the solid-state.[62] More recently, NMR crystallography structure determination protocols that combine experimental NMR data with density functional theory (DFT) calculations have been developed. Structure determination by NMR crystallography is usually accomplished by using crystal structure prediction (CSP)[63-69] to predict a large set of trial crystal structures. Plane-wave DFT calculations[54,70-72] are then used to calculate the ^{1}H and ^{13}C chemical shifts for the lowest energy trial structures.[54-56] Comparison of experimental and calculated chemical shifts allows identification of the trial crystal structure(s) that are in best agreement with the experimental structure.[54-56,58,73-75] Recently, modified NMR crystallography protocols that use genetic algorithms to generate trial structures and semi-empirical calculations of ^{1}H chemical shifts to test the trial structures were described.[59] Plane-wave DFT and solid-state NMR are also often applied to validate and/or refine structures determined by X-ray diffraction.[69,76-82]

The availability of high-field NMR systems and specialized pulse sequences has enabled solid-state NMR experiments on APIs with quadrupolar nuclei such as ^{7}Li,[83] ^{14}N,[84,85] ^{17}O,[86-90] ^{23}Na,[91,92] and ^{35}Cl.[93-96] For example, Schurko and co-workers have demonstrated that ^{35}Cl solid-state NMR spectroscopy can be applied to hydrochloride salts of APIs to differentiate polymorphs and detect APIs within dosage forms.[93-95] Wu and co-workers have previously applied ^{17}O solid-state NMR spectroscopy to study ^{17}O labeled pharmaceuticals such as acetylsalicylic acid (aspirin)[87] and warfarin.[90] Vogt used ^{17}O solid-state NMR, including 2D ^{1}H-^{17}O HETCOR experiments, to probe hydrogen bonding in several different solid forms of difflusinal.[88] Brown and co-workers have used ^{1}H-^{14}N double resonance solid-state NMR experiments to classify multicomponent solid APIs as salts or cocrystals and probe for interactions between APIs and polymers in amorphous dispersions.[84]

Solid-state NMR experiments on many APIs generally suffer from poor sensitivity due to a combination of effects such as long ^{1}H T_1, unfavorable nuclear properties (Table 1), peak splitting/broadening and the intrinsically low sensitivity of NMR spectroscopy. Consequently, solid-state NMR experiments on APIs are often restricted to basic 1D experiments on highly concentrated samples and receptive NMR-active nuclei (Table 1). This review describes how high-field dynamic nuclear polarization (DNP) can be applied to enhance the sensitivity of solid-state NMR experiments on pure and formulated APIs by several orders of magnitude.

The sensitivity gains provided by DNP enable advanced multi-dimensional NMR experiments to be performed with unreceptive NMR nuclei on both pure and formulated APIs, providing access to novel structural information about the molecular level and macroscopic structure of APIs.

Basic Aspects of High-Field Dynamic Nuclear Polarization. Here we give a brief overview of modern high-field DNP-enhanced solid-state NMR spectroscopy and instrumentation. The reader is referred to more thorough and comprehensive reviews and books on DNP.[98-101]

DNP was proposed by Overhauser in 1953 as a way to enhance nuclear spin polarization of NMR-active nuclei within metals.[102] DNP was experimentally demonstrated shortly thereafter by Carver and Slichter with ^{7}Li DNP solid-state NMR experiments on Li metal.[103] In a modern DNP experiment the large spin polarization of unpaired electrons is transferred to NMR-active nuclei, usually ^{1}H. Polarization transfer from the electrons to the NMR-active nuclei is typically achieved by saturating the electron paramagnetic resonance (EPR) at a specific frequency that depends upon the EPR properties of the polarizing agent (PA) and the DNP mechanism.[98-101] DNP-enhanced ^{1}H polarization can then be transferred to lower-γ heteronuclei such as ^{13}C or ^{15}N by using cross-polarization (CP) or other techniques. DNP can potentially enhance the polarization and sensitivity of NMR experiments that use ^{1}H nuclei by a factor of up to 658. Historically, DNP at high magnetic fields (5 T and above) was challenging due to the lack of high-power, high-frequency microwave sources. Due to the efforts of Griffin and co-workers,[98,99,104,105] and with the introduction of commercial DNP instrumentation (Figure 1)[106] it is now possible to routinely perform DNP-enhanced solid-state NMR at magnetic fields of up to 18.8 T. The commercial Bruker 9.4 T 263 GHz/400 MHz DNP solid-state NMR spectrometer[106] installed at the DOE Ames Laboratory is shown in Figure 1 and several of the system components are labeled.

There are three key concepts developed by Griffin and co-workers that have enabled large DNP signal enhancements to be routinely obtained at high magnetic fields.[98,99,104,105] First, a gyrotron provides the high-power microwaves that are required to saturate the EPR of the electrons and facilitate efficient polarization transfer to NMR-active nuclei.[104,106] A gyrotron is one of the few devices capable of producing high-power microwaves at frequencies above 200 GHz.[104-106] The microwaves are delivered into the low temperature MAS probe and up to the stator by the waveguide. Second, DNP-enhanced solid-state NMR experiments are performed at low temperatures by using cooled nitrogen gas for both MAS and sample cooling.[107] The electron relaxation times significantly increase at low temperature, enabling more complete saturation of the EPR and higher DNP

enhancements.[108] The nuclear relaxation times often increase as the sample temperature is reduced which also improves DNP enhancements. The cryogenic sample temperatures also bring other benefits such as improved performance of the probe electronics and increased thermal nuclear and electron polarization. Several research groups are currently exploring the possibility of using helium cooling to further reduce sample temperatures and obtain even larger DNP enhancements and higher absolute sensitivity.[109-112] Third, specially designed stable exogenous PA are introduced into the sample to provide a source of unpaired electrons for DNP.[113,114] Currently, the most efficient PA for MAS DNP are typically based upon biradicals (*e.g.*, TOTAPOL,[114] AMUPol,[115] TEKPol,[116] TEMTriPol[117]). The structures of the radical PA that currently provide the largest ^{1}H DNP enhancements are shown in Figure 2. At fields of 9.4 T and below, the optimized nitroxide biradical polarizing agents AMUPol[115] and TEKPol[116] can provide ^{1}H cross-effect (CE) DNP signal enhancements above 200. At magnetic fields above 9.4 T, the highest ^{1}H DNP signal enhancements have been obtained to date with a nitroxide-trityl biradical CE PA,[117] or with narrow line carbon centered mono-radicals such as BDPA that exploit the Overhauser Effect (OE).[118,119] The design and optimization of PA for high magnetic fields above 16.4 T is currently an active field of research. AMUPol, TEKPol and BDPA are all commercially available. Below we provide a practical description of how samples of organic solids and APIs are normally prepared for DNP solid-state NMR experiments.

Preparing Samples for DNP NMR Experiments.

A crucial aspect of DNP-enhanced solid-state NMR experiments is determining how to introduce ("dope") the exogenous PA into the sample of interest. The preparation of the sample has a large impact on both the DNP enhancements, nuclear relaxation rates and absolute sensitivity of the NMR experiments. Modern DNP solid-state NMR experiments on biomolecules or isotopically labeled small molecules are typically performed by dissolving or suspending the analyte in an aqueous radical solution (Figure 3A). Typically, partially deuterated water-glycerol solutions (glycerol-d_8/D_2O/H_2O, 60/30/10, v%), sometimes referred to as "DNP Juice", or partially deuterated dimethylsulfoxide-water solutions (DMSO-d_6/D_2O/H_2O, 60/36/4, v%) are used for DNP experiments on biomolecules.[114,121] The DMSO or glycerol act as cryoprotectants that prevent crystallization of the water and ensure that an amorphous glass is obtained upon freezing. Glass formation is critical to maintain a homogenous distribution of the PA and analytes and obtain a high DNP enhancement. However, solid-state NMR experiments on APIs are normally performed on microcrystalline solids, with the goal being to probe or determine the solid-state structure. Therefore, non-destructive methods of doping the sample with PA that avoid perturbing the solid-state structure of APIs are required.

Relayed DNP for Micro-Particulate APIs and Organic Solids. Relayed DNP experiments may be applied to polarize the ^{1}H nuclei inside of nano- or micro-particulate solids such as crystalline organic solids and APIs.[122,123] In a relayed DNP experiment a powdered solid is impregnated[124] with just enough radical solution to coat the outside of the particles (Figure 3B).[122,123] Upon microwave irradiation, DNP-enhanced ^{1}H polarization builds up at the surface of the particles and is continuously transported into the interior of the particle by ^{1}H spin diffusion.[122,123] In this way nano- or micro-particulate solids, such as APIs, can be remotely polarized. The DNP-enhanced ^{1}H polarization can then be transferred via CP[125] or other methods to the heteronuclei inside the particles.

The solvent for the radical solution that is used in the impregnation step must be carefully chosen to be a non-solvent for the solid material and should not perturb the solid-state structure of the analyte. Emsley and co-workers have previously identified several organic solvents that provide high DNP enhancements and are potentially compatible with relayed DNP.[126] Typically 1,1,2,2-tetrachloroethane (TCE) is the best organic solvent for relayed DNP experiments, however, TCE may dissolve or cause polymorphic phase transitions in some solids.[127] In such cases alternative solvents such as partially deuterated-

orthoterphenyl (OTP) [119,127-130], 1,3-dibromobutane (1,3-DBB) or 1,1,4,4-tetrabromoethane (TBE) may be used as solvents.[126] Notably, OTP has also allowed DNP enhancements of *ca.* 80 to be obtained with a high sample temperature of 240 K using TEKPol as the PA.[129] One other criteria for solvent selection is that the ^{13}C NMR signals of the solvent should not overlap with the analyte NMR signals, if possible. In cases where overlap with the solvent NMR signal is problematic, different solvent signal suppression methods based upon relaxation and/or dipolar couplings can be applied.[128,131] For example, pulse sequences with added spin echoes or spin-lock elements usually suppress the solvent signal.[128] Relayed DNP has been applied to many APIs and solids relevant to the pharmaceutical industry and the observed DNP signal enhancements are summarized in Table 2.[122,132,133] Jannin and co-workers have also demonstrated that relayed DNP can be used to polarize organic solids for dissolution DNP experiments.[134]

The DNP-enhanced ^{1}H, ^{13}C and ^{15}N solid-state NMR spectra of histidine hydrochloride monohydrate (histidine•HCl•H_2O) illustrate the sensitivity gains that can be achieved with relayed DNP (Figure 4). The primary factors that determine the magnitude of the DNP enhancements obtained in a relayed DNP experiment are the size of the particles and the ^{1}H T_1 of the ^{1}H nuclei inside of the particles, with smaller particles and longer ^{1}H T_1 leading to larger DNP enhancement (see below for a discussion of modeling the propagation of DNP-enhanced ^{1}H polarization by spin diffusion).[122,123] The sample of histidine•HCl•H_2O was prepared by finely grinding it by hand with a mortar and pestle to minimize the particle size and reduce the distance over which the DNP-enhanced ^{1}H polarization must be transported by ^{1}H spin diffusion. The finely ground powder was then impregnated with a 16 mM TEKPol TCE solution. Histidine•HCl•H_2O is an ideal setup compound for relayed DNP experiments because it has a very long ^{1}H T_1 at low temperatures, estimated to be greater than 200 s, and it is unaffected by sample grinding or impregnation with TCE. Histidine•HCl•H_2O also has favorable dielectric properties that increase the magnitude of the microwave fields across the rotor volume, resulting in large DNP enhancements.[132]

A large ^{1}H DNP enhancement (ε_H) of ca. 350 was measured with ^{1}H spin echo solid-state NMR spectra for the TCE at the surface of the histidine•HCl•H_2O particles (Figure 4). Measurement of the ^{13}C CPMAS DNP enhancement ($\varepsilon_{C\,CP}$) is performed by comparing the intensity of the ^{13}C solid-state NMR spectra acquired with and without microwave irradiation. For histidine•HCl•H_2O an $\varepsilon_{C\,CP}$ of 180 was measured with a recycle delay of 10.0 s. The $\varepsilon_{C\,CP}$ of 180 indicates that relayed DNP has increased the spin polarization of the ^{1}H nuclei inside of the histidine particles by more than two orders of magnitude. In relayed DNP experiments on microcrystalline solids the DNP enhancement for the ^{1}H nuclei in the interior of the

particles is normally lower than that observed for the ^{1}H nuclei of the solvent at the surface of the particles because some of the DNP-enhanced ^{1}H spin polarization is lost to longitudinal relaxation during the transport process.[122,123] With the gain in sensitivity provided by DNP it is possible to obtain natural isotopic abundance ^{13}C and ^{15}N solid-state NMR spectra with high signal-to-noise ratios in short experiment times; the ^{13}C solid-state NMR spectrum has a signal-to-noise ratio of ca. 700 after an 80 s experiment and the ^{15}N solid-state NMR spectrum has a signal-to-noise ratio of ca. 90 after an 8 minute experiment. The signal-to-noise ratios of the DNP-enhanced solid-state NMR spectra obtained with natural isotopic abundance are similar to that obtained with conventional solid-state NMR experiments on isotopically enriched samples. It is also important to note that the DNP-enhanced ^{13}C and ^{15}N solid-state NMR spectra of histidine•HCl•H_2O show good resolution with peak widths on the order of 0.7 ppm or less. This is significantly better resolution than is typically observed for DNP solid-state NMR spectra of analytes dissolved in glass-forming radical solutions where peak widths may be on the order of 1 ppm to 4 ppm. Relayed DNP experiments often result in high-resolution solid-state NMR spectra because the crystalline nature of the sample is unaffected by the sample preparation.[122,142]

One important issue to keep in mind when preparing samples for relayed DNP is that processes such as grinding, drying, impregnation and tablet compression may cause some organic solids and APIs to convert to different polymorphs or result in amorphous phases.[10,26] This is an important issue for the development of formulated pharmaceuticals because undesired API forms may reduce the efficacy of the formulation.[143] Recently, Emsley and co-workers demonstrated that both room temperature grinding and impregnation with non-solvents could cause phase transitions in some polymorphs and solvates of theophylline (Figure 5).[127] Therefore, care should be taken to ensure that the sample preparation steps of grinding and impregnation do not cause unwanted phase transitions when preparing samples for relayed DNP experiments. Polymorphic phase transitions can be easily monitored by comparing the ^{13}C solid-state NMR spectra of the pristine material to those of the materials subjected to grinding and/or impregnation with various solvents (Figure 5).[127] For form I of theophylline it was determined that phase transitions to other polymorphs could be prevented by grinding at reduced temperatures and using PA dissolved in a mixture of toluene and decalin for the impregnation step.[127] For some materials it may not be possible to use relayed DNP because the particle sizes are too large, the ^{1}H T_1 of the solid is too short (i.e., 2 s or less) or it is not possible to identify compatible DNP solvents that avoid phase transitions or dissolution. In such cases, direct-doping may be used to introduce the PA into the API.

Direct-Doping with PA. DNP-enhanced solid-state NMR spectroscopy has previously been performed on amorphous APIs, polymers, API-polymer mixtures (ASDs) and crystalline organic solids that were prepared by *directly* doping the analyte with the PA (Figure 3C). Direct-doping can be achieved in a couple of different ways. First, the PA may be introduced into the sample during the synthesis/precipitation of the material. Griffin and co-workers performed DNP-enhanced solid-state NMR on amorphous indomethacin obtained from hot melt extrusion.[130] The PA was introduced by directly dissolving it in the molten indomethacin during the melt extrusion process.[130] De Paëpe and co-workers performed DNP-enhanced solid-state NMR experiments on diphenylalanine nanotubes which were directly doped by adding the PA into the solution used to crystallize and grow the nanotubes.[144] Recently, Su and co-workers have incorporated PA into ASDs that were prepared either by spray drying or hot melt extrusion (Figure 6).[140] One obvious disadvantage of direct-doping is that the PA must be incorporated during synthesis/preparation of the sample.

Alternatively, it may be possible to post-synthetically directly dope the sample with PA by using solvents which swell or dissolve the solid material. For example, De Paëpe and co-workers performed DNP-enhanced solid-state NMR on cellulose which was impregnated/swollen with aqueous TOTAPOL solutions.[141] Viel and co-workers have performed DNP-enhanced solid-state NMR experiments on polymers that were either dissolved in glass-forming PA solutions or swollen with PA solution.[145] In both of these experiments, the sample partially dissolves or is swollen with the radical PA solution. A potential disadvantage of using a solvent that swells or dissolves the solid analyte is that it may perturb the solid-state structure. In all of these direct-doping methods it is also possible that there is some degree of phase segregation between the analyte and the PA, i.e., a case intermediate to that of Figure 3B and 3C. In such cases ^{1}H spin diffusion likely assists with the distribution of DNP-enhanced ^{1}H polarization. Finally, it is also important to keep in mind that in directly-doped samples most of the nuclei in the sample are in close proximity to PA molecules and the doping process may alter the structure of the solid. Therefore mechanisms such as signal broadening due to structural disorder, paramagnetic broadening/relaxation and MAS induced depolarization[146,147] may reduce the absolute sensitivity gains provided by DNP experiments on directly-doped samples.[122,141,148] On the other hand, direct-doping usually results in shorter, more favorable signal build-up times (T_B) because the radicals will be homogeneously distributed throughout the sample.

Modeling ^{1}H Spin Diffusion in Relayed DNP Experiments.

Models of ^{1}H spin diffusion have been widely applied in solid-state NMR spectroscopy to understand diverse phenomena such as enhanced longitudinal relaxation, mixing and segregation of solid phases, and to estimate the sizes of domains/particles.[44,122,123,149-156] Numerical and analytical models of ^{1}H spin diffusion can be used to obtain a fundamental understanding of the factors that determine the magnitude of the DNP enhancements in relayed DNP experiments.[122,123,155] As we describe in the applications section below, measurements of DNP enhancements can be combined with models of ^{1}H spin diffusion to estimate the diameter of API particles/domains within formulated pharmaceuticals.

The transport of DNP-enhanced polarization by ^{1}H spin diffusion in a heterogeneous system such as nano- or microparticles that are remotely polarized (Figure 3B) can be modeled with Fickian diffusion and described by the following differential equation:[123]

$$\frac{\partial P}{\partial t} = D(x)\Delta P - \frac{P(x,t) - P_0(x)}{T_1(x)} \quad (1)$$

where x is the position from the border (crystal surface) between the radical solution and the analyte, t the time, P the instantaneous polarization at position x and time t, P_0 the local equilibrium polarization level, D the diffusion rate at position x, T_1 the longitudinal relaxation time of the analyte at position x, and ΔP is the Laplacian of the polarization. The form of ΔP depends on the symmetry of the system. P_0 corresponds to the polarization that would be reached in the absence of spin diffusion. In the radical solution, the local equilibrium polarization without microwaves is the Boltzmann polarization, which is arbitrarily assigned a value of 1. With microwaves $P_0 = \varepsilon_0$ where ε_0 is the DNP enhancement of the solvent which is typically between 100 – 200. Inside of the analyte domains P_0 is always 1.

Griffin and co-workers used equation 1 to model relayed DNP in polypeptide nano-crystals suspended in a mixed water-glycerol solution with PA.[123] Assuming 1D symmetry, steady-state conditions (i.e., $\partial P / \partial t = 0$, realized at long polarization times) and by integrating the DNP signal enhancement over the 1D region, they obtained the following analytical expression for relayed DNP enhancement:

$$\varepsilon = \varepsilon_0 \frac{2\sqrt{DT_1}}{w} \tanh\left(\frac{w}{2\sqrt{DT_1}}\right) \quad (2)$$

In this equation ε is the integrated DNP enhancement inside of the remotely polarized 1D region, ε_0 is the DNP enhancement outside of the remotely polarized region (i.e., at the surface of a crystal), T_1 is the nuclear longitudinal relaxation time inside the polarized region, w is the width of the remotely polarized region and D is the spin diffusion rate, which is typically between 1×10^4 to 1×10^5 Å^2 s^{-1} in protonated organic solids. Equation (2) is very

useful for quickly estimating the expected magnitude of relayed DNP enhancements for different particle sizes and T_1 values. For example, equation 2 predicts that for a 2 μm wide 1D crystal, a ^{1}H T_1 of 100 s, a surface DNP enhancement (ε_0) of 100 and a spin diffusion rate of 1×10^5 Å^2 s^{-1} the integrated DNP enhancement observed inside the crystal would be a factor of 32 (i.e., 32% of the surface DNP enhancement). For the same conditions, but with T_1 = 10 s and T_1 = 1000 s equation 2 predicts the DNP enhancements inside the 1D crystal are 10 and 76, respectively. These examples illustrate that larger relayed DNP enhancements are obtained for solids with longer proton T_1. Proton T_1's on the order of hundreds of seconds are commonly observed for many organic solids and APIs,[122] especially at the cryogenic sample temperatures used for DNP experiments. All of the solids and APIs where relayed DNP has provided high DNP enhancements (Table 2) likely have long intrinsic proton T_1's that are greater than 30 s at 105 K.

Emsley and co-workers numerically solved equation (1) under assumptions of spherical symmetry in order to obtain a more detailed model of relayed DNP in microcrystalline solids and predict how relayed DNP affects relaxation and build-up of the NMR signal.[122] Equation (1) must be numerically solved to determine the instantaneous polarization [$P(x,t)$] as a function of position and time in a spherically symmetric system because there is no general analytical solution. Figure 7 illustrates the signal build-up rates and magnitude of the DNP enhancement predicted by numerically solving equation (1) assuming spherical particles and averaging the calculated polarization over position, particle volume and radius probability for several different particle radius distributions.[122] The spin diffusion model predicts that particles with smaller radii exhibit faster polarization build-up (Figure 7B) and larger DNP enhancements (Figure 7C), consequently, larger relayed DNP enhancements can be obtained for micro-particulate powders by grinding the sample to reduce the average particle size. The magnetization builds up more quickly for smaller particles because the signal build-up is primarily driven by diffusion of the DNP-enhanced magnetization into the particles. The rate of the signal build-up also depends upon the gradient of the polarization inside and outside the crystal, so that larger surface DNP enhancements should translate to faster signal build-ups and larger DNP enhancements inside the crystal. The spin diffusion model also predicts that the magnetization build-up can be fit with stretched exponential functions and that the apparent magnitude of the DNP enhancement will decrease as the polarization time is increased (Figure 7C). Both of these predictions have been confirmed by experiments.[122,133,155] Larger enhancements are obtained at shorter polarization times because the build-up of DNP-enhanced polarization at the surface of the particles accelerates the diffusion of polarization into the particles,

resulting in shorter signal build-up time constants in the DNP-enhanced NMR experiments as compared to the thermally polarized NMR experiments. Consequently, larger DNP enhancements are usually measured at short polarization delays and DNP enhancement usually decreases as the polarization time is increased in relayed DNP NMR experiments. Note that in glassy frozen solutions where the radical PA is homogeneously distributed the CE DNP enhancement usually shows no variation with the polarization delay.[155]

Figure 8 shows the steady-state DNP enhancements (ε_∞, the enhancement observed at long polarization times) predicted using numerical diffusion models for particles with different radii and for several different proton T_1's inside the crystals. This plot is useful to estimate the magnitude of the relayed DNP enhancement if the particle size and proton T_1 of the solid are known. Recently Pinon et al., have described phenomenological relations between ε_∞ and the radius of a spherical analyte (R):[155]

$$\varepsilon_\infty = 1 + \varepsilon_0 = 1 + \frac{3\sqrt{DT_1}}{R}\left[\coth\left(\frac{R}{\sqrt{DT_1}}\right) - \frac{\sqrt{DT_1}}{R}\right] \quad (3)$$

The definitions of the other terms in equation (3) are the same as those in equation (2). Phenomenological relationships between steady state enhancement and size of the remotely polarized analytes were also described for linear and cylindrical objects.[155] Equation (3) and/or Figure 8 can be used to estimate the particle radius for samples where the proton T_1 of the analyte, surface/solvent DNP enhancement and steady-state DNP enhancement for the analyte have been measured. The application of relayed DNP to determine particle/domain sizes is described in more detail in the applications section below.

Applications of DNP-Enhanced Solid-State NMR Spectroscopy to Pharmaceuticals

In this section we describe some of the advanced NMR experiments that have been performed with DNP on both pure and formulated APIs and emphasize the novel structural information provided by these experiments. Conventional solid-state NMR experiments on pure and formulated APIs are often hindered by poor sensitivity. Poor sensitivity typically limits NMR experiments to the acquisition of basic 1D ^{1}H and ^{13}C NMR experiments. DNP-enhanced solid-state NMR provides access to novel information about the molecular and macroscopic structure of pure and formulated APIs by enabling multi-dimensional NMR experiments that would normally be infeasible with conventional solid-state NMR spectroscopy. NMR experiments with unreceptive nuclei such as ^{14}N, ^{15}N and ^{35}Cl also become much more amenable with DNP.

Multi-dimensional Solid-State NMR Experiments on Pure APIs. Natural isotopic abundance double quantum-single quantum (DQ-SQ) ^{13}C-^{13}C homonuclear NMR experiments are frequently accelerated or enabled by DNP.[122,141] DQ homonuclear correlation NMR experiments provide valuable structural information because they allow resonances to be assigned, the chemical bonding/connectivity of atoms can be directly observed, internuclear distances can be measured and the relative orientations of the different NMR interaction tensors and local axes of functional groups can potentially be determined.[157-159] For example, ^{29}Si-^{29}Si and ^{31}P-^{31}P DQ-SQ correlation NMR experiments have previously been applied for structure determination of inorganic phosphates,[160] zeolites[161] and silica materials.[162] ^{13}C DQ NMR experiments on ^{13}C labeled samples have also been applied to determine torsion angles in organic solids and biomolecules.[163-165]

However, natural isotopic abundance ^{13}C homonuclear DQ NMR experiments typically require extremely long signal-averaging periods of days to weeks with conventional solid-state NMR spectroscopy.[58,159,166] The poor sensitivity arises because only 1 in 10000 carbon atoms exist as ^{13}C-^{13}C spin pairs that give rise to observable DQ NMR signal. However, with DNP both scalar and dipolar 2D^{13}C-^{13}C homonuclear correlation solid-state NMR experiments can be easily obtained with experiment times that are typically on the order of 12 hours or less.[122,141] For example, Emsley and co-workers applied relayed DNP to accelerate scalar and dipolar ^{13}C-^{13}C DQ-SQ homonuclear correlation spectra of organic solids such as glucose and sulfathiazole (Figure 9A).[122] In parallel, De Paëpe and co-workers applied DNP to cellulose swollen/impregnated with TOTAPOL to accelerate dipolar ^{13}C-^{13}C DQ-SQ correlation experiments.[141]

Dipolar DQ-SQ ^{13}C homonuclear solid-state NMR experiments can also be applied to estimate carbon-carbon internuclear distance and probe crystal packing. For example, Mollica et al. applied relayed DNP to theophylline to measure dipolar ^{13}C-^{13}C DQ-SQ correlation NMR spectra and measure DQ coherence signal build-up curves (Figure 9B).[139] The carbon-carbon internuclear distances from CSP trial structures of theophylline were then used to generate simulated analytical DQ build-up curves. Comparison of the predicted and experimental DQ build-up curves showed that the true crystal structure gave the best agreement with the observed DQ build-up curves, while the predicted DQ build-up curves for other polymorphs showed significantly worse agreement with the experimental curve. These findings suggested that ^{13}C-^{13}C DQ build-up curves are sensitive to molecular conformation and crystal packing and may be used to distinguish polymorphs and identify the correct structure amongst CSP trial structures.

De Paëpe and co-workers applied DNP-enhanced solid-state NMR to obtain dipolar ^{13}C-^{13}C DQ-SQ correlation NMR spectra and DQ build-up curves for diphenylalanine nanotubes that were directly doped with PA.[144,167] Using the carbon-carbon distances observed in the established crystal structure and with DFT calculated CS tensor orientations it was possible to reproduce the experimentally determined ^{13}C-^{13}C DQ build-up curves.[167] Notably, the DQ build-up curves could only be accurately simulated if carbon-carbon distances up to ca. 7 Å (dipolar couplings of ca. 20 Hz) were considered.[167] These results again highlight the sensitivity of dipolar DQ build-up curves to crystal packing and suggested that DQ-SQ ^{13}C-^{13}C NMR experiments can potentially be used to test the validity of proposed structural models. However, as noted by the authors, it is challenging to easily extract carbon-carbon distances from the observed DQ-build up curves because accurate simulation of the curve for a set of carbon resonances required knowledge of the CS tensors for each carbon and the relative orientations with respect to the other carbon atoms within the lattice. Additionally, multiple carbon-carbon dipolar couplings must be included in the simulations because there are multiple sets of carbon spin pairs due to the presence of adjacent, symmetry-related molecules within the crystal lattice.

DNP has also been applied to accelerate 2D heteronuclear correlation (HETCOR) solid-state NMR experiments. 2D ^{1}H-^{13}C and ^{1}H-^{15}N HETCOR experiments in conjunction with ^{1}H homonuclear decoupling sequences are widely employed to obtain high-resolution ^{1}H solid-state NMR spectra, measure heteronuclear dipolar couplings and perform resonance assignments in organic solids and APIs.[55,57,58,168-171] Conventional 2D ^{1}H-^{13}C HETCOR NMR experiments typically require experiment times of hours to days depending upon the characteristics of the sample, while 2D ^{1}H-^{15}N HETCOR NMR experiments are often infeasible with natural isotopic abundance. Relayed DNP has previously been used to rapidly acquire 2D ^{1}H-^{13}C and ^{1}H-^{15}N HETCOR solid-state NMR spectra of the API cetirizine hydrochloride[133] and of a self-assembled, oligomeric organic solid formed by reaction of CO_2 with amines.[172] With DNP 2D ^{1}H-^{13}C or ^{1}H-^{15}N HETCOR NMR spectra can typically be obtained in experiment times of minutes to a few hours, even in tablets which contain less than 10 wt.% API loading (see below).

Very recently, it has been demonstrated that conventional and DNP-enhanced 2D ^{1}H-^{13}C HETCOR NMR spectra can be used to significantly enhance the resolution of solid-state NMR spectra by reducing signal broadening from anisotropic bulk magnetic susceptibility (ABMS).[135] ABMS broadening frequently occurs in solids with aromatic groups and results in large inhomogeneous ^{1}H and ^{13}C line widths on the order of 1 to 2 ppm.[173,174] The low resolution caused by ABMS impedes the analysis of solid-state NMR spectra of APIs and organic solids. 2D HETCOR NMR spectra can reduce or eliminate inhomogeneous ABMS broadening because heteronuclear spin pairs experience the same local field,

resulting in elongated, elliptical cross-peaks due to correlated inhomogeneous broadening.[175] NMR spectra with improved resolution can then be extracted from the individual rows/columns of a 2D HETCOR spectrum.[175] For example, the ^{13}C solid-state NMR spectra of salicylic acid extracted from the rows of a DNP-enhanced 2D ^{1}H-^{13}C HETCOR spectrum obtained with ^{1}H homonuclear decoupling showed a factor 2.7 direct improvement in resolution as compared to the 1D ^{13}C CPMAS spectrum.[135] The direct gain in resolution depends upon the ratio of the ^{1}H and ^{13}C inhomogeneous linewidths to the ^{1}H homogeneous linewidth, which is determined by the efficiency of the homonuclear decoupling.[135] Conventional and DNP-enhanced 2D ^{1}H-^{13}C HETCOR NMR spectra were used to reduce ABMS broadening and resolve the overlapping NMR signals associated with the form 1 and form 2 polymorphs of aspirin within a mixture of both forms.[135] Therefore, in addition to the indirect gains in resolution achieved by adding a second spectral dimension, HETCOR experiments may provide further direct gains in resolution by reducing inhomogeneous ABMS broadening.

In addition to HETCOR experiments involving protons, DNP has also enabled acquisition of 2D HETCOR spectra that correlate moderate-γ and low-γ nuclei (e.g, ^{13}C-^{15}N, ^{13}C-^{14}N, ^{13}C-^{35}Cl, etc.). For instance, De Paëpe and co-workers recently applied relayed DNP to acquire natural isotopic abundance 2D ^{13}C-^{15}N dipolar HETCOR solid-state NMR spectra of a self-assembled 2′-deoxyguanosine derivative (Figure 9C).[176] This experiment is impossible to without DNP because with the natural isotopic abundance of ^{13}C and ^{15}N only 1 in 27000 carbon-nitrogen atom pairs will correspond to the ^{13}C-^{15}N isotopomer. 2D ^{13}C-^{15}N HETCOR solid-state NMR spectra could potentially be very informative probes of structure in APIs because they could be used for resonance assignment, resolution enhancement, carbon-nitrogen distance measurements and for mapping the connectivity/bonding of carbon and nitrogen atoms. In addition to correlations involving two spin-1/2 nuclei, DNP has also been used to correlate ^{13}C to quadrupolar nuclei. For example, Schurko and co-workers have recently demonstrated acquisition of a 2D $^{13}C\{^{35}Cl\}$ dipolar-HMQC correlation NMR spectrum of histidine•HCl•H_2O.[94] O'Dell and co-workers also applied relayed DNP to acquire 2D $^{13}C\{^{14}N$-overtone$\}$ correlation spectra.[137] Both of these results are discussed in more detail in the section describing DNP solid-state NMR experiments with quadrupolar nuclei.

DNP-Enhanced Solid-State NMR Experiments with Quadrupolar Nuclei. Another application of DNP is to enable and/or accelerate NMR experiments with quadrupolar nuclei such as ^{2}H, ^{14}N and ^{35}Cl. Approximately 73% of the spin active NMR isotopes in the periodic table are quadrupolar nuclei (nuclei with spin > ½). Some of the quadrupolar nuclei commonly encountered in APIs are listed in Table 1. Quadrupolar nuclei typically give rise to broad NMR signals because of broadening by the quadrupolar interaction (QI).[177-180] Useful

structural information may be obtained from the solid-state NMR spectra of quadrupolar nuclei because the broadening and appearance of the spectrum depends upon the spherical and rotational symmetry at the nuclear site.[177-180] However, signal broadening from the QI often leads to reduced sensitivity and poor resolution. By enhancing the nuclear spin polarization DNP can address the limitation of poor sensitivity. The resolution of solid-state NMR spectra of quadrupolar nuclei can be improved by adding a second spectral dimension that can resolve overlapping signals.

^{14}N is a spin-1 quadrupolar nucleus that is appealing for NMR experiments due to its high natural isotopic abundance of 99.6%. However, ^{14}N often gives rise to extremely broad (> 1 MHz) solid-state NMR spectra due to broadening by the first order QI. Consequently, direct acquisition of ^{14}N solid-state NMR spectra is typically performed on stationary samples with special CPMG based wideline solid-state NMR techniques.[181] The ^{14}N EFG tensor parameters determined in these experiments are useful for distinguishing polymorphs and probing the coordination environment/protonation state of the nitrogen atom.[85,182,183] However, the static wideline ^{14}N solid-state NMR experiments are often limited by poor sensitivity and resolution. As an alternative to static wideline experiments, fast MAS, proton detection and rotor synchronized HMQC pulse sequences may be used to detect ^{14}N solid-state NMR spectra indirectly.[184-186] Fast MAS $^{1}H\{^{14}N\}$ HMQC experiments have previously been applied to classify multicomponent solid APIs as salts or cocrystals and probe for interactions between APIs and polymers in an ASD.[84] Unfortunately, the efficiency of proton detected HMQC experiments is usually low when the nitrogen sites possess large quadrupolar coupling constants and/or when the ^{14}N nucleus is weakly coupled to ^{1}H. Bodenhausen and co-workers have previously applied DNP to enhance the sensitivity of 2D ^{13}C-^{14}N D-HMQC experiments on ^{13}C labeled proline dissolved in glass-forming PA solution.[187]

Overtone ^{14}N ($^{14}N^{OT}$) NMR has been demonstrated as a method to improve the resolution of ^{14}N solid-state NMR spectra.[188,189] In a $^{14}N^{OT}$ NMR experiment, the ^{14}N spins are irradiated and observed at twice the fundamental Larmor frequency of the ^{14}N nucleus. The MAS $^{14}N^{OT}$ solid-state NMR signals typically have widths of less than 10 kHz because the $^{14}N^{OT}$ NMR spectra are unaffected by the first-order QI.[190,191] Another advantage of $^{14}N^{OT}$ NMR is that MAS experiments are straightforward because the $^{14}N^{OT}$ spectrum is tolerant to deviations from the magic angle. Unfortunately, the $^{14}N^{OT}$ NMR experiments suffer from poor sensitivity because they require excitation of formally forbidden double quantum transitions.

In order to address these limitations O'Dell and co-workers applied relayed DNP to improve the sensitivity of $^{14}N^{OT}$ solid-state NMR experiments on microcrystalline amino acids (Figure 10).[137] They demonstrated that under MAS CP with short contact times could transfer DNP-enhanced ^{1}H polarization to the $^{14}N^{OT}$ transition. High-quality 1D ^{1}H-$^{14}N^{OT}$

CPMAS solid-state NMR spectra were typically obtained in about an hour with DNP. Notably, CP was found to provide similar or better excitation bandwidths than direct $^{14}N^{OT}$ excitation pulses. The observed $^{14}N^{OT}$ second-order quadrupolar MAS powder-patterns showed good agreement with numerically exact simulations,[191] and allowed the ^{14}N quadrupolar parameters to be accurately determined from fits of the spectra (Figure 10). However, comparison of DNP-enhanced 1D $^{14}N^{OT}$ and ^{15}N solid-state NMR spectra showed that ^{15}N NMR provides significantly better sensitivity than $^{14}N^{OT}$ NMR, despite the 270-fold lower isotopic abundance of ^{15}N in comparison to ^{14}N.[137] Therefore, the primary motivation for performing $^{14}N^{OT}$ NMR experiments is to obtain high-resolution measurements of ^{14}N EFG tensor parameters, rather than to improve sensitivity.

With DNP it was also possible to perform 2D $^{14}N^{OT}$ solid-state NMR experiments.[137] For example, a 2D ^{1}H-$^{14}N^{OT}$ CP-HETCOR spectrum with ^{1}H homonuclear decoupling applied in the indirect dimension allowed the overlapping $^{14}N^{OT}$ NMR signals of histidine•HCl•H_2O to be resolved on the basis of correlations to different ^{1}H NMR signals in the indirect dimension (Figure 10C). A DNP-enhanced 2D $^{13}C\{^{14}N^{OT}\}$ HMQC spectrum was obtained in a total experiment time of about 3.8 hours (Figure 10). The HMQC spectrum allowed overlapping $^{14}N^{OT}$ powder patterns to be resolved and the connectivity/bonding of the carbon and nitrogen atoms was determined. Note that 2D $^{13}C\{^{14}N^{OT}\}$ HMQC experiments had an efficiency of ca. 2.8% in comparison to a standard ^{13}C CPMAS spectrum. In comparison, natural abundance ^{13}C-^{15}N CP-HETCOR experiments can provide at most an efficiency of 0.37% (see above). Therefore, 2D $^{13}C\{^{14}N^{OT}\}$ or $^{13}C\{^{14}N\}$ HMQC is likely the highest sensitivity method to observe heteronuclear carbon and nitrogen correlations within natural isotopic abundance samples. However, 2D ^{13}C-^{15}N CP-HETCOR spectra will certainly provide better resolution and are more straightforward to interpret.

Hydrochloride salts of in both pure and dosage form can be studied with ^{35}Cl solid-state NMR spectroscopy.[93,95,96] ^{35}Cl solid-state NMR has previously been applied to differentiate the polymorphs of APIs and detect APIs within formulations.[93,95,96] ^{35}Cl is a highly abundant (NA = 75.5%) half-integer quadrupolar nucleus (I = 3/2). Due to broadening by the second-order QI the ^{35}Cl solid-state NMR spectra of hydrochloride salts are normally quite broad and acquisition is usually performed with static wideline CPMG techniques such as WCPMG or BRAIN-CP/WCPMG.[181] However, it may be challenging to obtain 1D ^{35}Cl solid-state NMR spectra of solids with unfavorable ^{1}H and ^{35}Cl relaxation times (long T_1's and short T_2 or $T_{1\rho}$) and/or in formulations where the loading of the API is low.

Schurko and co-workers applied relayed DNP to enhance the sensitivity of static ^{1}H-^{35}Cl BRAIN-CP/WCPMG experiments on both pure and formulated APIs (Figure 11).[94] They obtained ^{35}Cl CP DNP enhancements ($\varepsilon_{Cl\ CP}$) on the order of 7 to 100 from stationary

samples. The $\varepsilon_{Cl\,CP}$ obtained on static samples were between 3 to 8 times lower than those measured (with ^{13}C CPMAS experiments) on samples undergoing MAS. It was previously shown that the DNP enhancement obtained from nitroxide biradical PA are maximized with MAS frequencies between 2 to 8 kHz and that there was a large reduction in DNP enhancement for static samples.[106,116] The reduced enhancements for static samples likely occurred because there are fewer radicals in the proper orientation to participate in CE DNP. The magnitude of the DNP enhancements in the static solid-state NMR experiments was increased substantially by slowly spinning the sample (ca. 2 kHz MAS frequency) during the polarization delay, then the sample spinning was halted prior to applications of pulses and acquisition of the static NMR spectra.[94] This procedure was termed "spinning-on spinning-off" (SOSO). However, this procedure was only viable for samples with long proton T_1 where there was enough time to start and stop MAS during the polarization delays.

With the large sensitivity gains from DNP and BRAIN-CP/WCPMG, wideline ^{35}Cl solid-state NMR spectra of pure APIs were obtained in total experiment times of a few minutes.[94] Given the short experiment times on the pure APIs it was also possible to obtain DNP-enhanced ^{35}Cl solid-state NMR spectra of tables with low API loading (see below). Finally, a 2D ^{13}C{^{35}Cl} D-HMQC spectrum of histidine•HCl•H_2O was also acquired. This spectrum allowed the proximity of the ^{13}C and ^{35}Cl spins to be probed. 2D ^{13}C{^{35}Cl} D-HMQC experiments could be useful for samples which give rise to multiple overlapping ^{35}Cl NMR signals. The high-resolution ^{13}C dimension in a 2D D-HMQC spectrum could then be used to resolve the overlapping ^{35}Cl NMR signals. However, extension of this method to sites with larger ^{35}Cl quadrupolar coupling constants likely requires faster MAS frequencies greater than 40 kHz.[94]

^{2}H solid-state NMR is widely employed to obtain high-resolution hydrogen solid-state NMR spectra and probe dynamics by measurement of ^{2}H electric field gradient (EFG) tensors. ^{2}H NMR experiments are normally performed on ^{2}H labeled materials given its low 0.015% natural isotopic abundance. Relayed DNP was applied to theophylline and amino acids to obtain natural abundance MAS ^{2}H solid-state NMR spectra in experiment times on the order of one hour (Figure 12).[138] CP was used to transfer DNP-enhanced ^{1}H polarization to ^{2}H and the entire ^{2}H spinning sideband manifolds were uniformly excited. By fitting the MAS sideband manifolds observed in the ^{2}H solid-state NMR spectra it was possible to determine the ^{2}H EFG tensor parameters (C_Q and η_Q). With knowledge of C_Q and η_Q it was possible to correct the ^{2}H peak position for the quadrupole induced shift and determine the isotropic hydrogen chemical shift. Comparison of MAS ^{1}H solid-state NMR spectra obtained with the eDUMBO$_{1\text{-}22}$[192] and LG4[193] homonuclear decoupling sequences and MAS ^{2}H solid-state NMR spectra showed that both methods provided similar resolution. The hydrogen chemical shifts determined by both methods were also in good agreement. Therefore, natural abundance ^{2}H solid-state NMR spectroscopy was suggested an alternative method to ^{1}H homonuclear decoupling for acquisition of high-resolution hydrogen solid-state NMR spectra.

Characterization of Formulated APIs. Solid-state NMR spectroscopy is widely applied to determine and quantify the form of APIs within formulations.[143,194-196] However, the characterization of formulated APIs by solid-state NMR spectroscopy is often very challenging because of the dual problems of dilution and signal overlap. The API loading is often below 10 wt.% in formulations, which normally necessitates the use of long experiment times due to signal averaging.[143,194-196] Signal overlap occurs because the abundant

excipients give rise to intense ^{1}H and ^{13}C NMR signals that will either overwhelm or overlap with the signals from dilute API. One way to overcome these limitations is to use ^{13}C isotopically labeled APIs. For example, ^{13}C labeled steroid molecules could be detected at loadings as low as 0.5 wt.% in model formulations.[197] However, this approach requires synthesis of isotopically labeled materials and cannot be applied to analyze commercial products. DNP can directly address the problems of dilution and signal overlap, enabling low drug load formulations to be routinely studied by NMR with natural isotopic abundance. The large sensitivity enhancements provided by DNP can compensate any reductions in sensitivity due to dilution. Signal overlap can be addressed by performing 2D NMR experiments and/or observing the NMR spectra of elements such as nitrogen or chlorine that are likely only to be found within the API. Furthermore, by using numerical models of spin diffusion it is possible to use the measured DNP enhancements and signal build-up rates to probe the particle sizes of APIs within formulations.

Characterization of Commercial Tablets by DNP-Enhanced Solid-State NMR Spectroscopy. Emsley and co-workers applied relayed DNP to several different commercial tablets of the antihistamine drug cetirizine dihydrochloride.[133] The tablets had API loadings between 4.8 and 8.7 wt.%. The formulations were prepared for DNP experiments by breaking the tablet apart, then impregnating the powdered solid with a TEKPol TCE solution. Grinding of the tablet was not performed to avoid perturbing the particle size or phase of the different components. DNP-enhanced solid-state NMR experiments were also performed on the pure API and the individual excipients to measure the DNP enhancements and ^{13}C chemical shifts for each component of the tablet independently (Figure 13). Comparison of the ^{13}C solid-state NMR spectra of the excipients, pure APIs and the formulation allowed the different ^{13}C NMR signals of the tablet to be assigned. The ^{13}C solid-state NMR spectrum of the tablet indicated that the API was likely present as an amorphous form. Within the formulation the different components possessed different relayed DNP enhancements. The DNP enhancement was likely determined by the particle size and relaxation properties of each component. The largest DNP enhancements were obtained for the API and the excipient povidone. The similarity of the DNP enhancement of these two components suggested that they may be spatially proximate to one another and share a common bath of proton polarization. The high enhancement for the API was also beneficial because it helped to suppress the signals from the excipients in the DNP-enhanced NMR spectrum. The ^{13}C solid-state NMR spectrum of the tablet illustrates the problem of signal overlap; the chemical shifts of the different components coincide, which prevented resolution of the different signals.

DNP enables 2D NMR experiments and/or ^{15}N solid-state NMR experiments to be performed on tablets, solving the problem of signal overlap. For example, it was possible to obtain 2D ^{1}H-^{13}C CP-HETCOR spectra of the cetirizine tablets in experiment times of ca. 1 hour. The added dispersion provided by the ^{1}H dimension assisted in resolving the NMR signals from the different components. With the large sensitivity enhancements provided by DNP it was also possible to obtain 1D ^{15}N and 2D ^{1}H-^{15}N HETCOR solid-state NMR spectra (Figure 14). The 2D ^{1}H-^{15}N HETCOR NMR spectra were obtained in experiment times of less than 6 hours, despite the API loadings of less than 9 wt.%. Nitrogen NMR is advantageous because only the API and one of the excipients (povidone) contain nitrogen, eliminating the problem of overlap between the NMR signals from the API and excipients. Figure 14 compares the DNP-enhanced 2D ^{1}H-^{15}N CP-HETCOR spectra of crystalline API, amorphous API and a tablet which contains 8.7 wt.% API. This comparison confirms that the API was present as an amorphous form within the formulation. The 2D HETCOR spectra of the formulation showed that ^{15}N NMR signal at ca. 51.5 ppm correlated to the povidone ^{1}H NMR signal at a chemical shift of 1.4 ppm, which provided direct evidence for a molecular level interaction between povidone and the API. The interaction between povidone and the amorphous API is consistent with the fact that povidone is frequently used to form amorphous solid dispersions to stabilize amorphous APIs.

Schurko and co-workers have used DNP to obtain ^{35}Cl solid-state NMR spectra of APIs in commercial tablets with low API loadings.[94] Usually the API will be the only component within a formulation that contains chloride anions that can give rise to observable ^{35}Cl solid-state NMR signals. Therefore, ^{35}Cl solid-state NMR spectra of the tablets are free of interfering excipient signals and allow APIs to be directly interrogated.[94,95] For example, the DNP-enhanced static ^{35}Cl solid-state NMR spectra of pure crystalline diphenhydramine HCl and of a commercial tablet were identical in appearance, which confirmed that form of the API was identical in both the bulk and dosage form (Figure 11).[94] With the sensitivity enhancement provided by DNP and the BRAIN-CP/WCPMG pulse sequence it was generally possible to obtain ^{35}Cl solid-state NMR spectra in less than 12 hours from tablets with API loadings of less than 7 wt.%.

Determination of API Domain Sizes. Relaxation- and spin-diffusion solid-state NMR experiments have been broadly applied to probe the macroscopic structure and ordering/mixing within solid materials such as polymers.[154,156,198-200] In the context of pharmaceutical formulations, analysis of T_1 relaxation time constants, rotating-frame longitudinal relaxation times ($T_{1\rho}$) and spin-diffusion rates are commonly used to assess the

degree of mixing between excipients, polymers, coformers and APIs.[28,30,140,201,202] Here we describe how experimental measurements of relayed DNP enhancements and signal build-up rates can be fit to numerical models of spin diffusion (described above) to determine the particle/domain size of APIs within formulations. This method can potentially be applied to any kind of pharmaceutical formulation, with the only requirement being that there is phase segregation between the radical and the analyte and that the NMR signals from the analyte are resolved.

Rossini et al. analyzed the ^{13}C signal build-up rates and DNP enhancements with spin diffusion models in order to determine the particle/domain sizes of cetirizine dihydrochloride within commercial tablets.[133] Figure 15A shows the ^{13}C CPMAS signal build-up for the aromatic signals of the API obtained from saturation recovery experiments performed with and without microwaves to drive DNP (see Figure 13 for the corresponding ^{13}C solid-state NMR spectra of the tablet). The ^{1}H saturation recovery experiments were performed with ^{13}C signal detection in order to use the high-resolution ^{13}C dimension to resolve and differentiate the longitudinal ^{1}H relaxation rates associated with different components of the formulation. The ^{13}C signal build-up curves for the API could be fit to stretched exponential functions. Note that the signal build-up rate was observed to be accelerated with DNP. Both of these observations were consistent with the predictions of numerical spin diffusion simulations of relayed DNP. The DNP enhancement was determined for each polarization delay by dividing the signal intensity obtained with microwaves by the signal intensity without microwaves (Figure 15B). Figure 15C illustrates that povidone, which was hypothesized to coat the outside of the API particles, shows no clear variation in DNP enhancement with the polarization delay. The observed povidone DNP enhancement and measured relaxation times were incorporated into a numerical spin diffusion model which was used to predict the DNP enhancements as a function of the polarization delay for particles with different radii. Comparison of the observed DNP enhancements and the predicted enhancements for different particle sizes suggested that the API particles/domains had a radius of approximately 0.3 μm. Using the phenomenological equation (3) with $\varepsilon_0 = 43$, $\varepsilon_{analyte,\infty} = 23$, $T_{1,API} = 5.3$ s and $D = 10^5$ Å^2 s^{-1} gives a particle radius of 0.34 μm, in very good agreement with the value which was found with numerical simulations.

Relayed DNP NMR was also applied to determine the size of the ethycellulose (EC) and hydroxypropylcellulose (HPC) domains within blended films that are used in controlled release formulations.[155] The EC/HPC films were impregnated with a glycerol-d_8:D_2O:H_2O

(60:30:10 by volume %) solution with a 16 mM TOTAPOL concentration.[155] On the basis of observed enhancements and relaxation properties it was hypothesized that the PA solution penetrates and swells the amorphous HPC domains, while the PA does not enter the insoluble EC domains. The build-up of the polarization occured in the HPC domains and was relayed by spin diffusion into the EC domains. Therefore, by analyzing the DNP enhancements and signal build-up times it was possible to measure the size of the EC domains (Figure 16). Simulation of the variation in the relayed DNP enhancements with polarization time indicated that the length of the EC domains was 0.2 μm, in good agreement with measurements of the EC domain size made using paramagnetic relaxation enhancement.[154]

Characterization of Directly Doped Amorphous Solid Dispersions. An amorphous solid dispersion (ASD) consists of an amorphous API dissolved or suspended within a polymer matrix.[16-19] ASDs typically show superior drug solubility and bioavailability as compared to crystalline APIs.[16-19] Solid-state NMR is a powerful probe of structure in ASDs because it is possible to monitor phase segregation (crystallization of the API), measure API dynamics and probe for molecular level interactions between amorphous API and the polymer matrix.[30,143,201,203,204] Recently Su and co-workers have performed DNP-enhanced solid-state NMR experiments on ASDs that were directly doped by incorporating the PA during the spray drying or hot melt extrusion procedures that are used to prepare ASDs (Figure 6).[140] The advantage of the direct-doping method is that the PA is directly incorporated during synthesis; post-synthetic introduction of the PA into ASDs by swelling of the polymer matrix could potentially perturb the structure of the API/ASD.

Samples of the amorphous API clotrimazole, the polymer copovidone, and a clotrimazole-copovidone ASD were prepared for DNP experiments by directly adding TOTAPOL during hot melt extrusion or into the methanol solution used for spray drying.[140] The final concentration of the TOTAPOL PA in the solid materials was between 0.5 and 2 wt.%. DNP enhancements of 12, 4 and 5 were obtained for samples of clotrimazole, copovidone, and the ASD, respectively, all of which were prepared by spray drying. Samples prepared by hot melt extrusion exhibited similar DNP enhancements. For both spray drying and hot melt extrusion the largest DNP enhancements were typically obtained with final PA concentrations of ca. 1 wt.%. The proton T_1 of the spray-dried or extruded solids was also observed to substantially decrease with increasing radical concentration due to paramagnetic relaxation enhancement. DNP-enhanced NMR experiments were then performed on a posaconazole-^{2}H vinyl acetate ASD (ca. 20 wt % API) which was prepared by spray drying and contained 1 wt.% of AMUPOL (Figure 17). The use of deuterated vinyl acetate and AMUPOL resulted in a DNP enhancement of ca. 32 for the ASD, which was 3-4

times higher than the DNP enhancement measured for an ASD prepared with protonated polymer. With the large DNP enhancement it was possible to obtain 2D ^{1}H-^{13}C and ^{1}H-^{15}N HETCOR NMR spectra in experiment times of 7 hours (Figure 17). In summary, these results illustrate that direct-doping of an ASD can be achieved by incorporating the PA during spray drying or hot melt extrusion. Significant DNP enhancements can be obtained with this approach, enabling acquisition of 2D solid-state NMR spectra of ASDs.

Conclusions and Future Perspectives

This review has described how DNP-enhanced solid-state NMR may be applied for the characterization of APIs. Relayed DNP experiments can be applied to externally polarize microcrystalline solids. Numerical spin diffusion models describe the transport of DNP-enhanced polarization in samples with heterogeneous distributions of the PA. As an alternative to relayed DNP the PA may be directly doped into APIs during synthesis or crystallization. With modern DNP instrumentation and state-of-the-art designer PA it is possible to obtain routine DNP signal enhancements of 1 to 2 orders of magnitude in both pure and formulated APIs. The large gains in sensitivity provided by DNP enable solid-state NMR experiments which were previously very challenging or impossible. For example, with DNP it is possible to rapidly obtain homonuclear ^{13}C-^{13}C DQ-SQ correlation solid-state NMR spectra of pure organic solids and APIs. DNP has also permitted acquisition of ^{15}N and ^{35}Cl solid-state NMR spectra of formulated APIs with low drug loads. The ^{15}N and ^{35}Cl solid-state NMR spectra are free of interfering signals from excipients, allowing the API to be directly probed. Measurement of relayed DNP signal enhancements combined with numerical models of spin diffusion allowed the size of the API particles within tablets/formulations to be estimated. These examples demonstrate the unique insight into the molecular level and macroscopic structure of APIs that can potentially be obtained with DNP-enhanced solid-state NMR spectroscopy.

There are several interesting future directions for DNP-enhanced solid-state NMR experiments on APIs. First, high-field DNP is an emerging technique, with commercial instrumentation introduced only 7 years ago.[106] Currently, many research groups are developing hardware and polarization schemes to expand the capabilities of DNP and obtain further gains in absolute sensitivity. For example, helium-cooled systems allow MAS DNP experiments to be performed with sample temperatures of 50 K or less.[109-112] DNP at helium sample temperatures could likely provide a gain of 3 to 4 orders of magnitude in absolute sensitivity because DNP enhancements and Boltzmann polarization of the nuclear spins are both improved at lower temperatures. The development of next-generation microwave sources[136,205,206] could also bring about further substantial gains in sensitivity by enabling

pulsed DNP experiments[108,206-209] and electron decoupling.[210] The development of PA designed for OE DNP or biradical PA containing radicals with an isotropic EPR spectrum have allowed DNP enhancements greater than 50 to be obtained at magnetic fields above 16.4 T.[117,118] Probes capable of MAS at frequencies above 40 kHz have also been demonstrated.[119,211] Notably, fast MAS has allowed OE DNP enhancements of over 100 to be obtained at a high magnetic field of 18.8 T.[119] With fast MAS it should be possible to combine DNP and proton detection to obtain further improvements in resolution and absolute sensitivity.

Second, novel structural information obtained from DNP-enhanced solid-state NMR experiments will be implemented into NMR crystallography protocols to perform crystal structure determination/validation for both pure and formulated APIs. For example, the previously described DNP-enhanced homonuclear and heteronuclear correlation solid-state NMR experiments will provide access to novel structural constraints such as carbon-carbon and carbon-nitrogen interatomic distances.[122,141,144,167,172,176] Finally, we note that DNP has also been applied to obtain solid-state NMR spectra of unreceptive nuclei such as ^{17}O and ^{43}Ca found in inorganic materials.[212-214] We therefore expect that DNP should provide access to the natural isotopic abundance solid-state NMR spectra of unreceptive nuclei such as ^{17}O, ^{33}S and ^{43}Ca that are also commonplace in APIs. We speculate that with further gains in sensitivity provided by new DNP schemes and hardware, the types of experiments described here could one day be applied to perform *in situ* NMR crystallography on APIs in low drug load formulations.

Acknowledgements

This material is based upon work supported by the National Science Foundation under Grant No. 1709972 to AJR. AJR is also grateful for support from Genentech Inc., a subsidiary of Roche. AJR thanks Iowa State University and the Ames Laboratory (Royalty Account) for additional support. The Ames Laboratory is operated for the U.S. DOE by Iowa State University under contract no. DE-AC02-07CH11358. LE acknowledges ERC Advanced Grant No. 320860 and Swiss National Science Foundation Grant No. 200021_160112 for supporting this work. The authors thank their numerous co-authors and collaborators who have worked on the development of DNP NMR methods over the years.

References

[1] Hörter, D.; Dressman, J., *Adv. Drug Delivery Rev.* **1997**, *25*, 3.
[2] Chemburkar, S. R.; Bauer, J.; Deming, K.; Spiwek, H.; Patel, K.; Morris, J.; Henry, R.; Spanton, S.; Dziki, W.; Porter, W., *Org. Process Res. Dev.* **2000**, *4*, 413.
[3] Huang, L.-F.; Tong, W.-Q. T., *Adv. Drug Delivery Rev.* **2004**, *56*, 321.
[4] Bauer, J.; Morley, J.; Spanton, S.; Leusen, F.; Henry, R.; Hollis, S.; Heitmann, W.; Mannino, A.; Quick, J.; Dziki, W., *J. Pharm. Sci.* **2006**, *95*, 917.
[5] Hilfiker, R. *Polymorphism: in the pharmaceutical industry*; John Wiley & Sons, 2006.
[6] Braga, D.; Grepioni, F.; Maini, L.; Polito, M. In *Molecular Networks*; Hosseini, M. W., Ed.; Springer Berlin Heidelberg: Berlin, Heidelberg, 2009, p 87.
[7] Aitipamula, S.; Chow, P. S.; Tan, R. B., *CrystEngComm* **2014**, *16*, 3451.
[8] Brittain, H. G. *Polymorphism in pharmaceutical solids*; CRC Press, 2016.
[9] Lee, E. H., *Asian Journal of Pharmaceutical Sciences* **2014**, *9*, 163.
[10] Almarsson, Ö.; Zaworotko, M. J., *Chem. Commun.* **2004**, 1889.
[11] Aakeröy, C. B.; Fasulo, M. E.; Desper, J., *Mol. Pharm.* **2007**, *4*, 317.
[12] Childs, S. L.; Stahly, G. P.; Park, A., *Mol. Pharm.* **2007**, *4*, 323.
[13] Stahly, G. P., *Cryst. Growth Des.* **2007**, *7*, 1007.
[14] Friščić, T.; Jones, W., *J. Pharm. Pharmacol.* **2010**, *62*, 1547.
[15] Jones, W.; Motherwell, W. D. S.; Trask, A. V., *MRS Bulletin* **2011**, *31*, 875.
[16] Chiou, W. L.; Riegelman, S., *J. Pharm. Sci.* **1971**, *60*, 1281.
[17] Qian, F.; Huang, J.; Hussain, M. A., *J. Pharm. Sci.* **2010**, *99*, 2941.
[18] Newman, A.; Knipp, G.; Zografi, G., *J. Pharm. Sci.* **2012**, *101*, 1355.
[19] Baghel, S.; Cathcart, H.; O'Reilly, N. J., *J. Pharm. Sci.* **2016**, *105*, 2527.
[20] Singh, A.; Van den Mooter, G., *Adv. Drug Delivery Rev.* **2016**, *100*, 27.
[21] Bugay, D. E., *Pharm. Res.* **1993**, *10*, 317.
[22] Bugay, D. E., *Adv. Drug Delivery Rev.* **2001**, *48*, 43.
[23] Stephenson, G. A.; Forbes, R. A.; Reutzel-Edens, S. M., *Adv. Drug Delivery Rev.* **2001**, *48*, 67.
[24] Hancock, B. C.; Shalaev, E. Y.; Shamblin, S. L., *J. Pharm. Pharmacol.* **2002**, *54*, 1151.
[25] Reutzel-Edens, S.; Bush, J., *Am. Pharmaceut. Rev.* **2002**, *5*, 112.
[26] Tishmack, P. A.; Bugay, D. E.; Byrn, S. R., *J. Pharm. Sci.* **2003**, *92*, 441.
[27] Newman, A. W.; Byrn, S. R., *Drug Discov. Today* **2003**, *8*, 898.
[28] Lubach, J. W.; Munson, E. J. In *Encyclopedia of Analytical Chemistry*; John Wiley & Sons, Ltd: 2006.
[29] Harris, R. K., *J. Pharm. Pharmacol.* **2007**, *59*, 225.
[30] Geppi, M.; Mollica, G.; Borsacchi, S.; Veracini, C. A., *Appl. Spectrosc. Rev.* **2008**, *43*, 202.
[31] Berendt, R. T.; Sperger, D. M.; Munson, E. J.; Isbester, P. K., *TrAC Trends in Analytical Chemistry* **2006**, *25*, 977.
[32] Harris, R. K., *Analyst* **2006**, *131*, 351.
[33] Vogt, F. G., *Future* **2010**, *2*, 915.
[34] Bakeev, K. A. *Process analytical technology: spectroscopic tools and implementation strategies for the chemical and pharmaceutical industries*; John Wiley & Sons, 2010.
[35] Holzgrabe, U. *NMR spectroscopy in pharmaceutical analysis*; Elsevier, 2011.
[36] Jimenez-Barbero, J.; Waterton, J.; Vogt, F. G. *New applications of NMR in drug discovery and development*; Royal Society of Chemistry, 2013.
[37] Pindelska, E.; Sokal, A.; Kolodziejski, W., *Adv. Drug Delivery Rev.* **2017**, *117*, 111.
[38] Ripmeester, J. A., *Chem. Phys. Lett.* **1980**, *74*, 536.
[39] Fletton, R. A.; Harris, R. K.; Kenwright, A. M.; Lancaster, R. W.; Packer, K. J.; Sheppard, N., *Spectrochimica Acta Part A: Molecular Spectroscopy* **1987**, *43*, 1111.
[40] Byrn, S. R.; Sutton, P. A.; Tobias, B.; Frye, J.; Main, P., *J. Am. Chem. Soc.* **1988**, *110*, 1609.

[41] Brittain, H. G.; Morris, K. R.; Bugay, D. E.; Thakur, A. B.; Serajuddin, A. T., *J. Pharm. Biomed. Anal.* **1993**, *11*, 1063.
[42] Apperley, D. C.; Fletton, R. A.; Harris, R. K.; Lancaster, R. W.; Tavener, S.; Threlfall, T. L., *J. Pharm. Sci.* **1999**, *88*, 1275.
[43] Harris, R. K., *Solid State Sci.* **2004**, *6*, 1025.
[44] Lubach, J. W.; Xu, D.; Segmuller, B. E.; Munson, E. J., *J. Pharm. Sci.* **2007**, *96*, 777.
[45] Schantz, S.; Hoppu, P.; Juppo, A., *J. Pharm. Sci.* **2009**, *98*, 1862.
[46] Zhou, D. H.; Rienstra, C. M., *Angew. Chem. Int. Ed.* **2008**, *47*, 7328.
[47] Spiess, H. W. In *eMagRes* 2012.
[48] Pandey, M. K.; Kato, H.; Ishii, Y.; Nishiyama, Y., *Phys. Chem. Chem. Phys.* **2016**, *18*, 6209.
[49] Zhang, R.; Mroue, K. H.; Ramamoorthy, A., *Acc. Chem. Res.* **2017**, *50*, 1105.
[50] Salager, E.; Stein, R. S.; Steuernagel, S.; Lesage, A.; Elena, B.; Emsley, L., *Chem. Phys. Lett.* **2009**, *469*, 336.
[51] Ryan, L.; Taylor, R.; Paff, A.; Gerstein, B., *J. Chem. Phys.* **1980**, *72*, 508.
[52] Elena, B.; Emsley, L., *J. Am. Chem. Soc.* **2005**, *127*, 9140.
[53] Griffin, J. M.; Martin, D. R.; Brown, S. P., *Angew. Chem. Int. Ed.* **2007**, *46*, 8036.
[54] Pickard, C. J.; Salager, E.; Pintacuda, G.; Elena, B.; Emsley, L., *J. Am. Chem. Soc.* **2007**, *129*, 8932.
[55] Salager, E.; Stein, R. S.; Pickard, C. J.; Elena, B.; Emsley, L., *Phys. Chem. Chem. Phys.* **2009**, *11*, 2610.
[56] Salager, E.; Day, G. M.; Stein, R. S.; Pickard, C. J.; Elena, B.; Emsley, L., *J. Am. Chem. Soc.* **2010**, *132*, 2564.
[57] Mafra, L.; Santos, S. M.; Siegel, R.; Alves, I.; Almeida Paz, F. A.; Dudenko, D.; Spiess, H. W., *J. Am. Chem. Soc.* **2012**, *134*, 71.
[58] Baias, M.; Widdifield, C. M.; Dumez, J.-N.; Thompson, H. P. G.; Cooper, T. G.; Salager, E.; Bassil, S.; Stein, R. S.; Lesage, A.; Day, G. M.; Emsley, L., *Phys. Chem. Chem. Phys.* **2013**, *15*, 8069.
[59] Santos, S. M.; Rocha, J.; Mafra, L., *Cryst. Growth Des.* **2013**, *13*, 2390.
[60] Maruyoshi, K.; Iuga, D.; Watts, A. E.; Hughes, C. E.; Harris, K. D. M.; Brown, S. P., *J. Pharm. Sci.* **2017**, DOI:10.1016/j.xphs.2017.07.014.
[61] Elena, B.; Pintacuda, G.; Mifsud, N.; Emsley, L., *J. Am. Chem. Soc.* **2006**, *128*, 9555.
[62] Seidel, K.; Etzkorn, M.; Sonnenberg, L.; Griesinger, C.; Sebald, A.; Baldus, M., *J. Phys. Chem. A* **2005**, *109*, 2436.
[63] Lommerse, J. P. M.; Motherwell, W. D. S.; Ammon, H. L.; Dunitz, J. D.; Gavezzotti, A.; Hofmann, D. W. M.; Leusen, F. J. J.; Mooij, W. T. M.; Price, S. L.; Schweizer, B.; Schmidt, M. U.; van Eijck, B. P.; Verwer, P.; Williams, D. E., *Acta Crystallographica Section B* **2000**, *56*, 697.
[64] Day, G. M.; Motherwell, W. D. S.; Ammon, H. L.; Boerrigter, S. X. M.; Della Valle, R. G.; Venuti, E.; Dzyabchenko, A.; Dunitz, J. D.; Schweizer, B.; van Eijck, B. P.; Erk, P.; Facelli, J. C.; Bazterra, V. E.; Ferraro, M. B.; Hofmann, D. W. M.; Leusen, F. J. J.; Liang, C.; Pantelides, C. C.; Karamertzanis, P. G.; Price, S. L.; Lewis, T. C.; Nowell, H.; Torrisi, A.; Scheraga, H. A.; Arnautova, Y. A.; Schmidt, M. U.; Verwer, P., *Acta Crystallographica Section B* **2005**, *61*, 511.
[65] Motherwell, W. D. S.; Ammon, H. L.; Dunitz, J. D.; Dzyabchenko, A.; Erk, P.; Gavezzotti, A.; Hofmann, D. W. M.; Leusen, F. J. J.; Lommerse, J. P. M.; Mooij, W. T. M.; Price, S. L.; Scheraga, H.; Schweizer, B.; Schmidt, M. U.; van Eijck, B. P.; Verwer, P.; Williams, D. E., *Acta Crystallographica Section B* **2002**, *58*, 647.
[66] Day, G. M.; Cooper, T. G.; Cruz-Cabeza, A. J.; Hejczyk, K. E.; Ammon, H. L.; Boerrigter, S. X. M.; Tan, J. S.; Della Valle, R. G.; Venuti, E.; Jose, J.; Gadre, S. R.; Desiraju, G. R.; Thakur, T. S.; van Eijck, B. P.; Facelli, J. C.; Bazterra, V. E.; Ferraro, M. B.; Hofmann, D. W. M.; Neumann, M. A.; Leusen, F. J. J.; Kendrick, J.; Price, S. L.; Misquitta, A. J.; Karamertzanis, P. G.; Welch, G. W. A.; Scheraga, H. A.; Arnautova, Y. A.; Schmidt, M. U.; van de Streek, J.; Wolf, A. K.; Schweizer, B., *Acta Crystallographica Section B* **2009**, *65*, 107.

[67] Reilly, A. M.; Cooper, R. I.; Adjiman, C. S.; Bhattacharya, S.; Boese, A. D.; Brandenburg, J. G.; Bygrave, P. J.; Bylsma, R.; Campbell, J. E.; Car, R.; Case, D. H.; Chadha, R.; Cole, J. C.; Cosburn, K.; Cuppen, H. M.; Curtis, F.; Day, G. M.; DiStasio Jr, R. A.; Dzyabchenko, A.; van Eijck, B. P.; Elking, D. M.; van den Ende, J. A.; Facelli, J. C.; Ferraro, M. B.; Fusti-Molnar, L.; Gatsiou, C.-A.; Gee, T. S.; de Gelder, R.; Ghiringhelli, L. M.; Goto, H.; Grimme, S.; Guo, R.; Hofmann, D. W. M.; Hoja, J.; Hylton, R. K.; Iuzzolino, L.; Jankiewicz, W.; de Jong, D. T.; Kendrick, J.; de Klerk, N. J. J.; Ko, H.-Y.; Kuleshova, L. N.; Li, X.; Lohani, S.; Leusen, F. J. J.; Lund, A. M.; Lv, J.; Ma, Y.; Marom, N.; Masunov, A. E.; McCabe, P.; McMahon, D. P.; Meekes, H.; Metz, M. P.; Misquitta, A. J.; Mohamed, S.; Monserrat, B.; Needs, R. J.; Neumann, M. A.; Nyman, J.; Obata, S.; Oberhofer, H.; Oganov, A. R.; Orendt, A. M.; Pagola, G. I.; Pantelides, C. C.; Pickard, C. J.; Podeszwa, R.; Price, L. S.; Price, S. L.; Pulido, A.; Read, M. G.; Reuter, K.; Schneider, E.; Schober, C.; Shields, G. P.; Singh, P.; Sugden, I. J.; Szalewicz, K.; Taylor, C. R.; Tkatchenko, A.; Tuckerman, M. E.; Vacarro, F.; Vasileiadis, M.; Vazquez-Mayagoitia, A.; Vogt, L.; Wang, Y.; Watson, R. E.; de Wijs, G. A.; Yang, J.; Zhu, Q.; Groom, C. R., *Acta Crystallographica Section B* **2016**, *72*, 439.
[68] Hartman, J. D.; Day, G. M.; Beran, G. J., *Cryst. Growth Des.* **2016**, *16*, 6479.
[69] Widdifield, C. M.; Robson, H.; Hodgkinson, P., *Chem. Commun.* **2016**, *52*, 6685.
[70] Hohenberg, P.; Kohn, W., *Phys. Rev.* **1964**, *136*, B864.
[71] Charpentier, T., *Solid State Nucl. Magn. Reson.* **2011**, *40*, 1.
[72] Bonhomme, C.; Gervais, C.; Babonneau, F.; Coelho, C.; Pourpoint, F.; Azaïs, T.; Ashbrook, S. E.; Griffin, J. M.; Yates, J. R.; Mauri, F., *Chem. Rev* **2012**, *112*, 5733.
[73] Sardo, M.; Siegel, R.; Santos, S. M.; Rocha, J.; Gomes, J. R. B.; Mafra, L., *J. Phys. Chem. A* **2012**, *116*, 6711.
[74] Kalakewich, K.; Iuliucci, R.; Harper, J. K., *Cryst. Growth Des.* **2013**, *13*, 5391.
[75] Ashbrook, S. E.; McKay, D., *Chem. Commun.* **2016**, *52*, 7186.
[76] Harper, J. K.; Iuliucci, R.; Gruber, M.; Kalakewich, K., *CrystEngComm* **2013**, *15*, 8693.
[77] Pawlak, T.; Potrzebowski, M. J., *J. Phys. Chem. B* **2014**, *118*, 3298.
[78] Kalakewich, K.; Iuliucci, R.; Mueller, K. T.; Eloranta, H.; Harper, J. K., *The Journal of Chemical Physics* **2015**, *143*, 194702.
[79] Kerr, H. E.; Mason, H. E.; Sparkes, H. A.; Hodgkinson, P., *CrystEngComm* **2016**, *18*, 6700.
[80] Dudek, M. K.; Bujacz, G.; Potrzebowski, M. J., *CrystEngComm* **2017**, *19*, 2903.
[81] Hofstetter, A.; Emsley, L., *J. Am. Chem. Soc.* **2017**, *139*, 2573.
[82] Widdifield, C. M.; Nilsson Lill, S. O.; Broo, A.; Lindkvist, M.; Pettersen, A.; Svensk Ankarberg, A.; Aldred, P.; Schantz, S.; Emsley, L., *Phys. Chem. Chem. Phys.* **2017**, *19*, 16650.
[83] Haimovich, A.; Eliav, U.; Goldbourt, A., *J. Am. Chem. Soc.* **2012**, *134*, 5647.
[84] Tatton, A. S.; Pham, T. N.; Vogt, F. G.; Iuga, D.; Edwards, A. J.; Brown, S. P., *Mol. Pharm.* **2013**, *10*, 999.
[85] Veinberg, S. L.; Johnston, K. E.; Jaroszewicz, M. J.; Kispal, B. M.; Mireault, C. R.; Kobayashi, T.; Pruski, M.; Schurko, R. W., *Phys. Chem. Chem. Phys.* **2016**, *18*, 17713.
[86] Pike, K. J.; Lemaître, V.; Kukol, A.; Anupold, T.; Samoson, A.; Howes, A. P.; Watts, A.; Smith, M. E.; Dupree, R., *J. Phys. Chem. B* **2004**, *108*, 9256.
[87] Kong, X.; Shan, M.; Terskikh, V.; Hung, I.; Gan, Z.; Wu, G., *J. Phys. Chem. B* **2013**, *117*, 9643.
[88] Vogt, F. G.; Yin, H.; Forcino, R. G.; Wu, L., *Mol. Pharm.* **2013**, *10*, 3433.
[89] Wu, G., *Solid State Nucl. Magn. Reson.* **2016**, *73*, 1.
[90] Kong, X.; Dai, Y.; Wu, G., *Solid State Nucl. Magn. Reson.* **2017**, *84*, 59.
[91] Burgess, K.; Perras, F. A.; Lebrun, A.; Messner-Henning, E.; Korobkov, I.; Bryce, D. L., *J. Pharm. Sci.* **2012**, *101*, 2930.
[92] Dicaire, N. M.; Perras, F. A.; Bryce, D. L., *Can. J. Chem.* **2013**, *92*, 9.
[93] Hamaed, H.; Pawlowski, J. M.; Cooper, B. F.; Fu, R.; Eichhorn, S. H.; Schurko, R. W., *J. Am. Chem. Soc.* **2008**, *130*, 11056.
[94] Hirsh, D. A.; Rossini, A. J.; Emsley, L.; Schurko, R. W., *Phys. Chem. Chem. Phys.* **2016**, *18*, 25893.

[95] Namespetra, A. M.; Hirsh, D. A.; Hildebrand, M. P.; Sandre, A. R.; Hamaed, H.; Rawson, J. M.; Schurko, R. W., *CrystEngComm* **2016**, *18*, 6213.
[96] Hildebrand, M.; Hamaed, H.; Namespetra, A. M.; Donohue, J. M.; Fu, R.; Hung, I.; Gan, Z.; Schurko, R. W., *CrystEngComm* **2014**, *16*, 7334.
[97] Harris, R. K.; Becker, E. D.; Cabral de Menezes, S. M.; Goodfellow, R.; Granger, P., *Magn. Reson. Chem.* **2002**, *40*, 489.
[98] Barnes, A. B.; Paëpe, G. D.; van der Wel, P. C. A.; Hu, K. N.; Joo, C. G.; Bajaj, V. S.; Mak-Jurkauskas, M. L.; Sirigiri, J. R.; Herzfeld, J.; Temkin, R. J.; Griffin, R. G., *Appl. Magn. Reson.* **2008**, *34*, 237.
[99] Ni, Q. Z.; Daviso, E.; Can, T. V.; Markhasin, E.; Jawla, S. K.; Swager, T. M.; Temkin, R. J.; Herzfeld, J.; Griffin, R. G., *Acc. Chem. Res.* **2013**, *46*, 1933.
[100] Kuhn, L. T.; Akbey, Ü. *Hyperpolarization methods in NMR spectroscopy*; Springer, 2013; Vol. 338.
[101] Thankamony, A. S. L.; Wittmann, J. J.; Kaushik, M.; Corzilius, B., *Prog. Nucl. Magn. Reson. Spectrosc.* **2017**,
[102] Overhauser, A. W., *Phys. Rev.* **1953**, *92*, 411.
[103] Carver, T. R.; Slichter, C. P., *Phys. Rev.* **1953**, *92*, 212.
[104] Becerra, L. R.; Gerfen, G. J.; Temkin, R. J.; Singel, D. J.; Griffin, R. G., *Phys. Rev. Lett.* **1993**, *71*, 3561.
[105] Maly, T.; Debelouchina, G. T.; Bajaj, V. S.; Hu, K.-N.; Joo, C.-G.; Mak–Jurkauskas, M. L.; Sirigiri, J. R.; van der Wel, P. C.; Herzfeld, J.; Temkin, R. J., *J. Chem. Phys.* **2008**, *128*, 02B611.
[106] Rosay, M.; Tometich, L.; Pawsey, S.; Bader, R.; Schauwecker, R.; Blank, M.; Borchard, P. M.; Cauffman, S. R.; Felch, K. L.; Weber, R. T., *Phys. Chem. Chem. Phys.* **2010**, *12*, 5850.
[107] Hall, D. A.; Maus, D. C.; Gerfen, G. J.; Inati, S. J.; Becerra, L. R.; Dahlquist, F. W.; Griffin, R. G., *Science* **1997**, *276*, 930.
[108] Can, T. V.; Ni, Q. Z.; Griffin, R. G., *J. Magn. Reson.* **2015**, *253*, 23.
[109] Thurber, K. R.; Yau, W.-M.; Tycko, R., *J. Magn. Reson.* **2010**, *204*, 303.
[110] Matsuki, Y.; Ueda, K.; Idehara, T.; Ikeda, R.; Ogawa, I.; Nakamura, S.; Toda, M.; Anai, T.; Fujiwara, T., *J. Magn. Reson.* **2012**, *225*, 1.
[111] Bouleau, E.; Saint-Bonnet, P.; Mentink-Vigier, F.; Takahashi, H.; Jacquot, J. F.; Bardet, M.; Aussenac, F.; Purea, A.; Engelke, F.; Hediger, S.; Lee, D.; De Paepe, G., *Chem. Sci.* **2015**, *6*, 6806.
[112] Thurber, K.; Tycko, R., *J. Magn. Reson.* **2016**, *264*, 99.
[113] Hu, K.-N.; Yu, H.-h.; Swager, T. M.; Griffin, R. G., *J. Am. Chem. Soc.* **2004**, *126*, 10844.
[114] Song, C.; Hu, K.-N.; Joo, C.-G.; Swager, T. M.; Griffin, R. G., *J. Am. Chem. Soc.* **2006**, *128*, 11385.
[115] Sauvée, C.; Rosay, M.; Casano, G.; Aussenac, F.; Weber, R. T.; Ouari, O.; Tordo, P., *Angew. Chem. Int. Ed.* **2013**, *125*, 11058.
[116] Zagdoun, A.; Casano, G.; Ouari, O.; Schwarzwälder, M.; Rossini, A. J.; Aussenac, F.; Yulikov, M.; Jeschke, G.; Copéret, C.; Lesage, A.; Tordo, P.; Emsley, L., *J. Am. Chem. Soc.* **2013**, *135*, 12790.
[117] Mathies, G.; Caporini, M. A.; Michaelis, V. K.; Liu, Y.; Hu, K.-N.; Mance, D.; Zweier, J. L.; Rosay, M.; Baldus, M.; Griffin, R. G., *Angew. Chem. Int. Ed.* **2015**, *54*, 11770.
[118] Can, T. V.; Caporini, M. A.; Mentink-Vigier, F.; Corzilius, B.; Walish, J. J.; Rosay, M.; Maas, W. E.; Baldus, M.; Vega, S.; Swager, T. M.; Griffin, R. G., *J. Chem. Phys.* **2014**, *141*, 064202.
[119] Chaudhari, S. R.; Wisser, D.; Pinon, A. C.; Berruyer, P.; Gajan, D.; Tordo, P.; Ouari, O.; Reiter, C.; Engelke, F.; Copéret, C.; Lelli, M.; Lesage, A.; Emsley, L., *J. Am. Chem. Soc.* **2017**, *139*, 10609.
[120] Koelsch, C. F., *J. Am. Chem. Soc.* **1957**, *79*, 4439.
[121] Matsuki, Y.; Maly, T.; Ouari, O.; Karoui, H.; Le Moigne, F.; Rizzato, E.; Lyubenova, S.; Herzfeld, J.; Prisner, T.; Tordo, P.; Griffin, R. G., *Angew. Chem. Int. Ed.* **2009**, *48*, 4996.

[122] Rossini, A. J.; Zagdoun, A.; Hegner, F.; Schwarzwalder, M.; Gajan, D.; Coperet, C.; Lesage, A.; Emsley, L., *J. Am. Chem. Soc.* **2012**, *134*, 16899.
[123] van der Wel, P. C.; Hu, K.-N.; Lewandowski, J.; Griffin, R. G., *J. Am. Chem. Soc.* **2006**, *128*, 10840.
[124] Lesage, A.; Lelli, M.; Gajan, D.; Caporini, M. A.; Vitzthum, V.; Miéville, P.; Alauzun, J.; Roussey, A.; Thieuleux, C.; Mehdi, A.; Bodenhausen, G.; Coperet, C.; Emsley, L., *J. Am. Chem. Soc.* **2010**, *132*, 15459.
[125] Pines, A.; Gibby, M.; Waugh, J., *Chem. Phys. Lett.* **1972**, *15*, 373.
[126] Zagdoun, A.; Rossini, A. J.; Gajan, D.; Bourdolle, A.; Ouari, O.; Rosay, M.; Maas, W. E.; Tordo, P.; Lelli, M.; Emsley, L.; Lesage, A.; Coperet, C., *Chem. Commun.* **2012**, *48*, 654.
[127] Pinon, A. C.; Rossini, A. J.; Widdifield, C. M.; Gajan, D.; Emsley, L., *Mol. Pharmaceutics* **2015**, *12*, 4146.
[128] Yarava, J. R.; Chaudhari, S. R.; Rossini, A. J.; Lesage, A.; Emsley, L., *J. Magn. Reson.* **2017**, *277*, 149.
[129] Lelli, M.; Chaudhari, S. R.; Gajan, D.; Casano, G.; Rossini, A. J.; Ouari, O.; Tordo, P.; Lesage, A.; Emsley, L., *J. Am. Chem. Soc.* **2015**, *137*, 14558.
[130] Ong, T.-C.; Mak-Jurkauskas, M. L.; Walish, J. J.; Michaelis, V. K.; Corzilius, B.; Smith, A. A.; Clausen, A. M.; Cheetham, J. C.; Swager, T. M.; Griffin, R. G., *J. Phys. Chem. B* **2013**, *117*, 3040.
[131] Lee, D.; Chaudhari, S. R.; De Paëpe, G., *J. Magn. Reson.* **2017**, *278*, 60.
[132] Kubicki, D. J.; Rossini, A. J.; Purea, A.; Zagdoun, A.; Ouari, O.; Tordo, P.; Engelke, F.; Lesage, A.; Emsley, L., *J. Am. Chem. Soc.* **2014**, *136*, 15711.
[133] Rossini, A. J.; Widdifield, C. M.; Zagdoun, A.; Lelli, M.; Schwarzwalder, M.; Coperet, C.; Lesage, A.; Emsley, L., *J. Am. Chem. Soc.* **2014**, *136*, 2324.
[134] Ji, X.; Bornet, A.; Vuichoud, B.; Milani, J.; Gajan, D.; Rossini, A. J.; Emsley, L.; Bodenhausen, G.; Jannin, S., *Nat. Commun.* **2017**, *8*, 13975.
[135] Hanrahan, M. P.; Venkatesh, A.; Carnahan, S. L.; Calahan, J. L.; Lubach, J. W.; Munson, E. J.; Rossini, A. J., *Phys. Chem. Chem. Phys.* **2017**, *19*, 28153
[136] Kemp, T. F.; Dannatt, H. R. W.; Barrow, N. S.; Watts, A.; Brown, S. P.; Newton, M. E.; Dupree, R., *J. Magn. Reson.* **2016**, *265*, 77.
[137] Rossini, A. J.; Emsley, L.; O'Dell, L. A., *Phys. Chem. Chem. Phys.* **2014**, *16*, 12890.
[138] Rossini, A. J.; Schlagnitweit, J.; Lesage, A.; Emsley, L., *J. Magn. Reson.* **2015**, *259*, 192.
[139] Mollica, G.; Dekhil, M.; Ziarelli, F.; Thureau, P.; Viel, S., *Angew. Chem., Int. Ed.* **2015**, *54*, 6028.
[140] Ni, Q. Z.; Yang, F.; Can, T. V.; Sergeyev, I. V.; D'Addio, S. M.; Jawla, S. K.; Li, Y.; Lipert, M. P.; Xu, W.; Williamson, R. T.; Leone, A.; Griffin, R. G.; Su, Y., *J. Phys. Chem. B* **2017**, *121*, 8132.
[141] Takahashi, H.; Lee, D.; Dubois, L.; Bardet, M.; Hediger, S.; De Paëpe, G., *Angew. Chem. Int. Ed.* **2012**, *51*, 11766.
[142] Barnes, A. B.; Corzilius, B.; Mak-Jurkauskas, M. L.; Andreas, L. B.; Bajaj, V. S.; Matsuki, Y.; Belenky, M. L.; Lugtenburg, J.; Sirigiri, J. R.; Temkin, R. J., *Phys. Chem. Chem. Phys.* **2010**, *12*, 5861.
[143] Lubach, J.; Padden, B.; Winslow, S.; Salsbury, J.; Masters, D.; Topp, E.; Munson, E., *Anal. Bioanal. Chem.* **2004**, *378*, 1504.
[144] Takahashi, H.; Viverge, B.; Lee, D.; Rannou, P.; De Paëpe, G., *Angew. Chem. Int. Ed.* **2013**, *52*, 6979.
[145] Le, D.; Casano, G.; Phan, T. N. T.; Ziarelli, F.; Ouari, O.; Aussenac, F.; Thureau, P.; Mollica, G.; Gigmes, D.; Tordo, P.; Viel, S., *Macromolecules* **2014**, *47*, 3909.
[146] Thurber, K. R.; Tycko, R., *J. Chem. Phys.* **2014**, *140*, 184201.
[147] Mentink-Vigier, F.; Akbey, Ü.; Hovav, Y.; Vega, S.; Oschkinat, H.; Feintuch, A., *J. Magn. Reson.* **2012**, *224*, 13.
[148] Rossini, A. J.; Zagdoun, A.; Lelli, M.; Gajan, D.; Rascón, F.; Rosay, M.; Maas, W. E.; Copéret, C.; Lesage, A.; Emsley, L., *Chem. Sci.* **2012**, *3*, 108.
[149] Bloembergen, N., *Physica* **1949**, *15*, 386.

[150] Rorschach, H., *Physica* **1964**, *30*, 38.
[151] Tse, D.; Lowe, I., *Phys. Rev.* **1968**, *166*, 292.
[152] Brownstein, K. R.; Tarr, C. E., *Phys. Rev. A* **1979**, *19*, 2446.
[153] Bertini, I.; Luchinat, C.; Parigi, G. *Solution NMR of paramagnetic molecules: applications to metallobiomolecules and models*; Elsevier, 2001; Vol. 2.
[154] Schlagnitweit, J.; Tang, M.; Baias, M.; Richardson, S.; Schantz, S.; Emsley, L., *J. Am. Chem. Soc.* **2015**, *137*, 12482.
[155] Pinon, A. C.; Schlagnitweit, J.; Berruyer, P.; Rossini, A. J.; Lelli, M.; Socie, E.; Tang, M.; Pham, T.; Lesage, A.; Schantz, S., *The Journal of Physical Chemistry C* **2017**, *121*, 15993.
[156] Schmidt-Rohr, K.; Spiess, H. W. *Multidimensional solid-state NMR and polymers*; Academic Press, 1994.
[157] Feng, X.; Verdegem, P. J. E.; Edén, M.; Sandström, D.; Lee, Y. K.; Bovee-Geurts, P. H. M.; de Grip, W. J.; Lugtenburg, J.; de Groot, H. J. M.; Levitt, M. H., *Journal of Biomolecular NMR* **2000**, *16*, 1.
[158] Lesage, A.; Bardet, M.; Emsley, L., *J. Am. Chem. Soc.* **1999**, *121*, 10987.
[159] De Paëpe, G.; Lesage, A.; Steuernagel, S.; Emsley, L., *ChemPhysChem* **2004**, *5*, 869.
[160] Dollase, W. A.; Feike, M.; Förster, H.; Schaller, T.; Schnell, I.; Sebald, A.; Steuernagel, S., *J. Am. Chem. Soc.* **1997**, *119*, 3807.
[161] Brouwer, D. H.; Darton, R. J.; Morris, R. E.; Levitt, M. H., *J. Am. Chem. Soc.* **2005**, *127*, 10365.
[162] Brouwer, D. H.; Cadars, S.; Eckert, J.; Liu, Z.; Terasaki, O.; Chmelka, B. F., *J. Am. Chem. Soc.* **2013**, *135*, 5641.
[163] Feng, X.; Lee, Y. K.; Sandstrom, D.; Eden, M.; Maisel, H.; Sebald, A.; Levitt, M., *Chem. Phys. Lett.* **1996**, *257*, 314.
[164] Schmidt-Rohr, K., *J. Am. Chem. Soc.* **1996**, *118*, 7601.
[165] Feng, X.; Verdegem, P.; Lee, Y.; Sandström, D.; Edén, M.; Bovee-Geurts, P.; De Grip, W.; Lugtenburg, J.; De Groot, H.; Levitt, M., *J. Am. Chem. Soc.* **1997**, *119*, 6853.
[166] Harris, R. K.; Joyce, S. A.; Pickard, C. J.; Cadars, S.; Emsley, L., *Phys. Chem. Chem. Phys.* **2006**, *8*, 137.
[167] Marker, K.; Paul, S.; Fernandez-de-Alba, C.; Lee, D.; Mouesca, J. M.; Hediger, S.; De Paepe, G., *Chemical Science* **2017**, *8*, 974.
[168] van Rossum, B. J.; de Groot, C. P.; Ladizhansky, V.; Vega, S.; de Groot, H. J. M., *J. Am. Chem. Soc.* **2000**, *122*, 3465.
[169] Vogt, F. G.; Clawson, J. S.; Strohmeier, M.; Edwards, A. J.; Pham, T. N.; Watson, S. A., *Cryst. Growth Des.* **2009**, *9*, 921.
[170] Liu, W.; Wang, W. D.; Wang, W.; Bai, S.; Dybowski, C., *J. Phys. Chem. B* **2010**, *114*, 16641.
[171] Abraham, A.; Apperley, D. C.; Byard, S. J.; Ilott, A. J.; Robbins, A. J.; Zorin, V.; Harris, R. K.; Hodgkinson, P., *CrystEngComm* **2016**, *18*, 1054.
[172] Leclaire, J.; Poisson, G.; Ziarelli, F.; Pepe, G.; Fotiadu, F.; Paruzzo, F. M.; Rossini, A. J.; Dumez, J.-N.; Elena-Herrmann, B.; Emsley, L., *Chem. Sci.* **2016**, *7*, 4379.
[173] Vanderhart, D. L.; Earl, W. L.; Garroway, A. N., *J. Magn. Reson.* **1981**, *44*, 361.
[174] Barich, D. H.; Davis, J. M.; Schieber, L. J.; Zell, M. T.; Munson, E. J., *J. Pharm. Sci.* **2006**, *95*, 1586.
[175] Kervern, G.; Pintacuda, G.; Zhang, Y.; Oldfield, E.; Roukoss, C.; Kuntz, E.; Herdtweck, E.; Basset, J. M.; Cadars, S.; Lesage, A.; Coperet, C.; Emsley, L., *J. Am. Chem. Soc.* **2006**, *128*, 13545.
[176] Märker, K.; Pingret, M.; Mouesca, J.-M.; Gasparutto, D.; Hediger, S.; De Paëpe, G., *J. Am. Chem. Soc.* **2015**, *137*, 13796.
[177] Kentgens, A. P. M., *Geoderma* **1997**, *80*, 271.
[178] Ashbrook, S. E.; Duer, M. J., *Concepts in Magnetic Resonance Part A* **2006**, *28A*, 183.
[179] Ashbrook, S. E., *Phys. Chem. Chem. Phys.* **2009**, *11*, 6892.
[180] Wasylishen, R. E.; Ashbrook, S. E.; Wimperis, S. *NMR of quadrupolar nuclei in solid materials*; John Wiley & Sons, 2012.
[181] Schurko, R. W., *Acc. Chem. Res.* **2013**, *46*, 1985.

[182] O'Dell, L. A.; Schurko, R. W.; Harris, K. J.; Autschbach, J.; Ratcliffe, C. I., *J. Am. Chem. Soc.* **2010**, *133*, 527.
[183] Veinberg, S. L.; Friedl, Z. W.; Harris, K. J.; O'Dell, L. A.; Schurko, R. W., *CrystEngComm* **2015**, *17*, 5225.
[184] Gan, Z., *J. Am. Chem. Soc.* **2006**, *128*, 6040.
[185] Cavadini, S.; Lupulescu, A.; Antonijevic, S.; Bodenhausen, G., *J. Am. Chem. Soc.* **2006**, *128*, 7706.
[186] Cavadini, S.; Abraham, A.; Bodenhausen, G., *Chem. Phys. Lett.* **2007**, *445*, 1.
[187] Vitzthum, V.; Caporini, M. A.; Bodenhausen, G., *J. Magn. Reson.* **2010**, *205*, 177.
[188] Bloom, M.; LeGros, M. A., *Can. J. Phys.* **1986**, *64*, 1522.
[189] Tycko, R.; Opella, S., *J. Chem. Phys.* **1987**, *86*, 1761.
[190] O'Dell, L. A.; Ratcliffe, C. I., *Chem. Phys. Lett.* **2011**, *514*, 168.
[191] O'Dell, L. A.; Brinkmann, A., *J. Chem. Phys.* **2013**, *138*, 064201.
[192] Elena, B.; de Paëpe, G.; Emsley, L., *Chem. Phys. Lett.* **2004**, *398*, 532.
[193] Halse, M. E.; Emsley, L., *J. Phys. Chem. A* **2013**, *117*, 5280.
[194] Saindon, P. J.; Cauchon, N. S.; Sutton, P. A.; Chang, C.-J.; Peck, G. E.; Byrn, S. R., *Pharm. Res.* **1993**, *10*, 197.
[195] Katrincic, L. M.; Sun, Y. T.; Carlton, R. A.; Diederich, A. M.; Mueller, R. L.; Vogt, F. G., *Int. J. Pharm.* **2009**, *366*, 1.
[196] Harris, R. K.; Hodgkinson, P.; Larsson, T.; Muruganantham, A., *J. Pharm. Biomed. Anal.* **2005**, *38*, 858.
[197] Booy, K. J.; Wiegerinck, P.; Vader, J.; Kaspersen, F.; Lambregts, D.; Vromans, H.; Kellenbach, E., *J. Pharm. Sci.* **2005**, *94*, 458.
[198] Clauss, J.; Schmidt-Rohr, K.; Spiess, H. W., *Acta Polym.* **1993**, *44*, 1.
[199] Demco, D. E.; Johansson, A.; Tegenfeldt, J., *Solid State Nucl. Magn. Reson.* **1995**, *4*, 13.
[200] VanderHart, D. L.; McFadden, G. B., *Solid State Nucl. Magn. Reson.* **1996**, *7*, 45.
[201] Vogt, F. G.; Williams, G. R., *Pharm. Res.* **2012**, *29*, 1866.
[202] Pham, T. N.; Watson, S. A.; Edwards, A. J.; Chavda, M.; Clawson, J. S.; Strohmeier, M.; Vogt, F. G., *Mol. Pharm.* **2010**, *7*, 1667.
[203] Paudel, A.; Geppi, M.; Mooter, G. V. d., *J. Pharm. Sci.* **2014**, *103*, 2635.
[204] Song, Y.; Yang, X.; Chen, X.; Nie, H.; Byrn, S.; Lubach, J. W., *Mol. Pharm.* **2015**, *12*, 857.
[205] Kim, H. J.; Nanni, E. A.; Shapiro, M. A.; Sirigiri, J. R.; Woskov, P. P.; Temkin, R. J., *Phys. Rev. Lett.* **2010**, *105*, 135101.
[206] Hoff, D. E. M.; Albert, B. J.; Saliba, E. P.; Scott, F. J.; Choi, E. J.; Mardini, M.; Barnes, A. B., *Solid State Nucl. Magn. Reson.* **2015**, *72*, 79.
[207] Henstra, A.; Dirksen, P.; Schmidt, J.; Wenckebach, W. T., *Journal of Magnetic Resonance (1969)* **1988**, *77*, 389.
[208] Mathies, G.; Jain, S.; Reese, M.; Griffin, R. G., *The Journal of Physical Chemistry Letters* **2016**, *7*, 111.
[209] Can, T. V.; Weber, R. T.; Walish, J. J.; Swager, T. M.; Griffin, R. G., *Angewandte Chemie International Edition* **2017**, *56*, 6744.
[210] Saliba, E. P.; Sesti, E. L.; Scott, F. J.; Albert, B. J.; Choi, E. J.; Alaniva, N.; Gao, C.; Barnes, A. B., *J. Am. Chem. Soc.* **2017**, *139*, 6310.
[211] Chaudhari, S. R.; Berruyer, P.; Gajan, D.; Reiter, C.; Engelke, F.; Silverio, D. L.; Coperet, C.; Lelli, M.; Lesage, A.; Emsley, L., *Phys. Chem. Chem. Phys.* **2016**, *18*, 10616.
[212] Blanc, F.; Sperrin, L.; Jefferson, D. A.; Pawsey, S.; Rosay, M.; Grey, C. P., *J. Am. Chem. Soc.* **2013**, *135*, 2975.
[213] Perras, F. A.; Kobayashi, T.; Pruski, M., *J. Am. Chem. Soc.* **2015**, *137*, 8336.
[214] Lee, D.; Leroy, C.; Crevant, C.; Bonhomme-Coury, L.; Babonneau, F.; Laurencin, D.; Bonhomme, C.; De Paepe, G., *Nat. Commun.* **2017**, *8*, 14104.

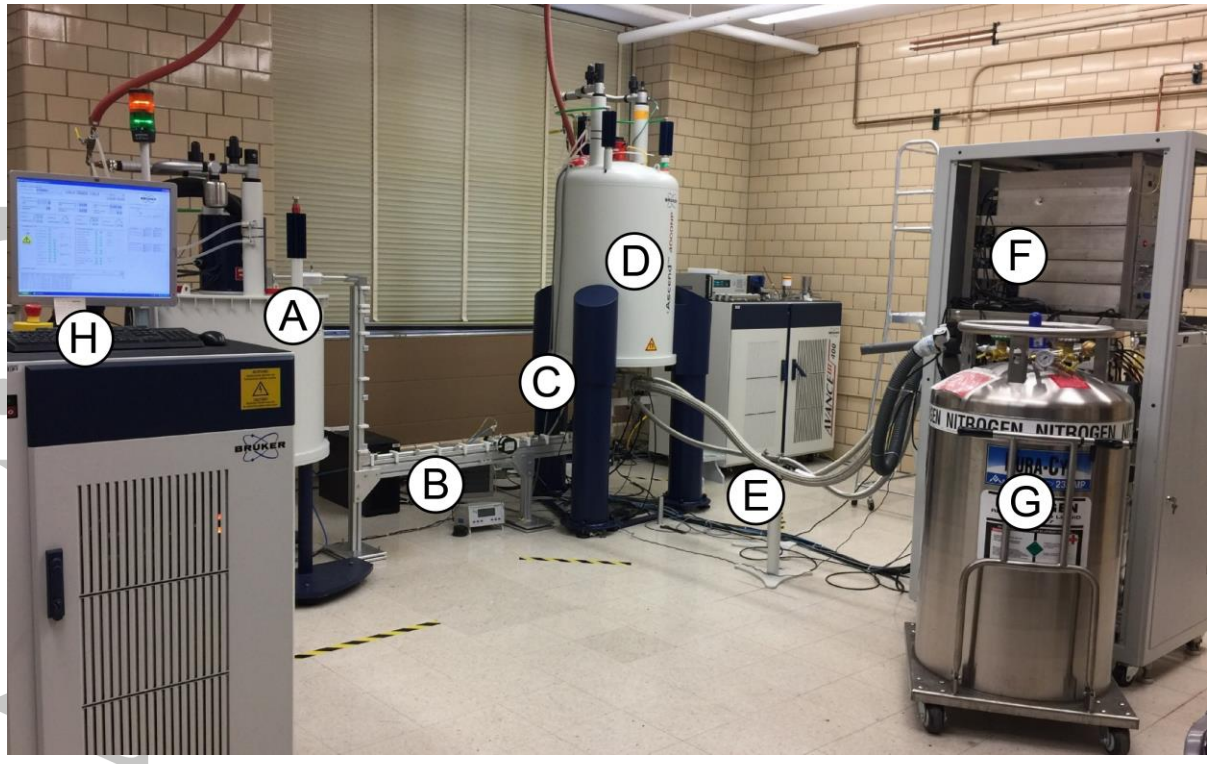

Figure 1. The commercial Bruker 9.4 T/263 GHz DNP solid-state NMR spectrometer[106] setup at the Ames Laboratory. 263 GHz continuous wave microwaves are generated by a gyrotron (A) and transmitted via the transmission line (B) to the MAS probe (C) housed in the 9.4 T widebore NMR magnet (D). Sample temperatures of *ca.* 100 K are achieved by using cold nitrogen gas for sample spinning and sample cooling. The cold nitrogen gas is delivered to the MAS probe in an insulated transfer line (E). The nitrogen gas is cooled inside of a pressurized heat exchanger (F) which is fed with liquid nitrogen (G). The gyrotron control computer (H) can be used to turn the continuous wave 263 GHz microwaves on or off and adjust the microwave power.

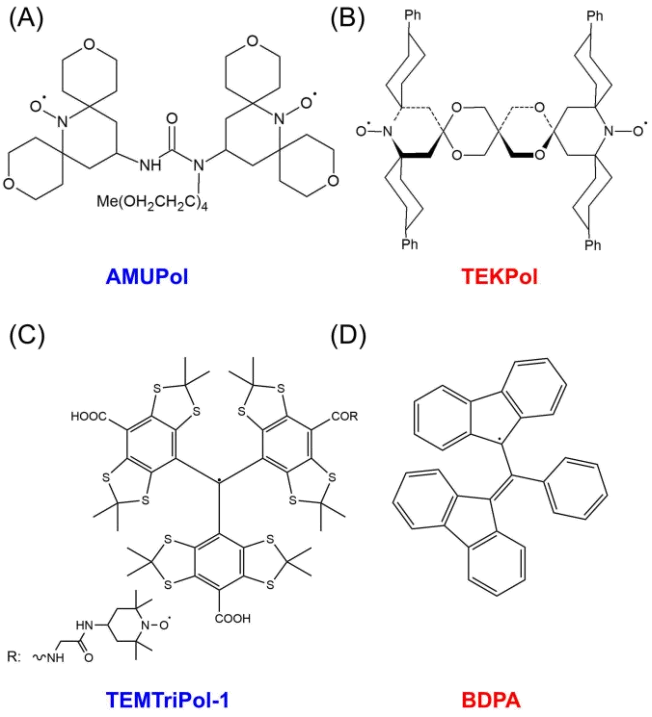

Figure 2. The molecular structures of exogenous DNP polarizing agents (PA). (A) AMUPol[115] (B), TEKPol[116] (C) TEMTriPol-1[117] and (D) BDPA.[120] The CE polarizing agents AMUPol and TEKPol typically provide the largest ^{1}H DNP signal enhancements at fields of 9.4 T or lower. AMUPol is used with aqueous solvent mixtures, while TEKPol is used with organic solvents. TEMTriPol-1 and BDPA have provided the largest ^{1}H DNP enhancements at magnetic fields of 16.4 T and higher.

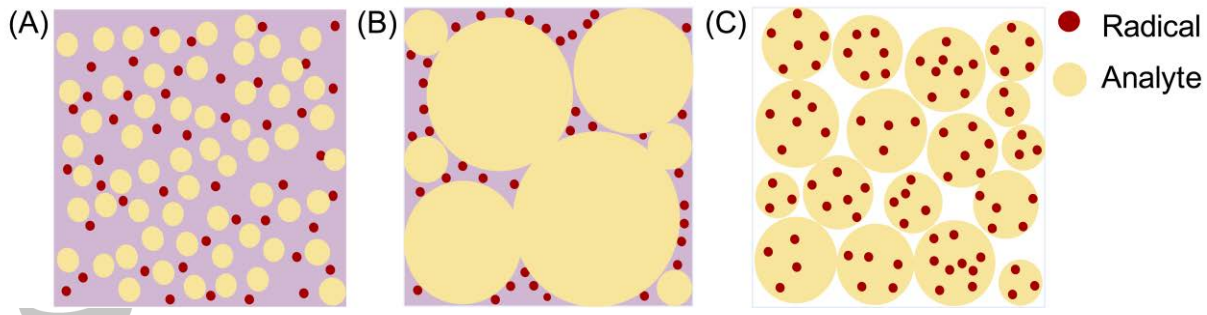

Figure 3. Cartoons of DNP sample preparations illustrating the distribution of analyte (yellow spheres) and radical PA (red spheres). (A) The analyte is dissolved and homogenously distributed in the radical containing solution, (B) An inhomogeneous nano- or micro-particulate analyte is impregnated with a radical solution and the PA is restricted to the surface of the analyte domains; (C) Direct-doping of the PA into the analyte particles.

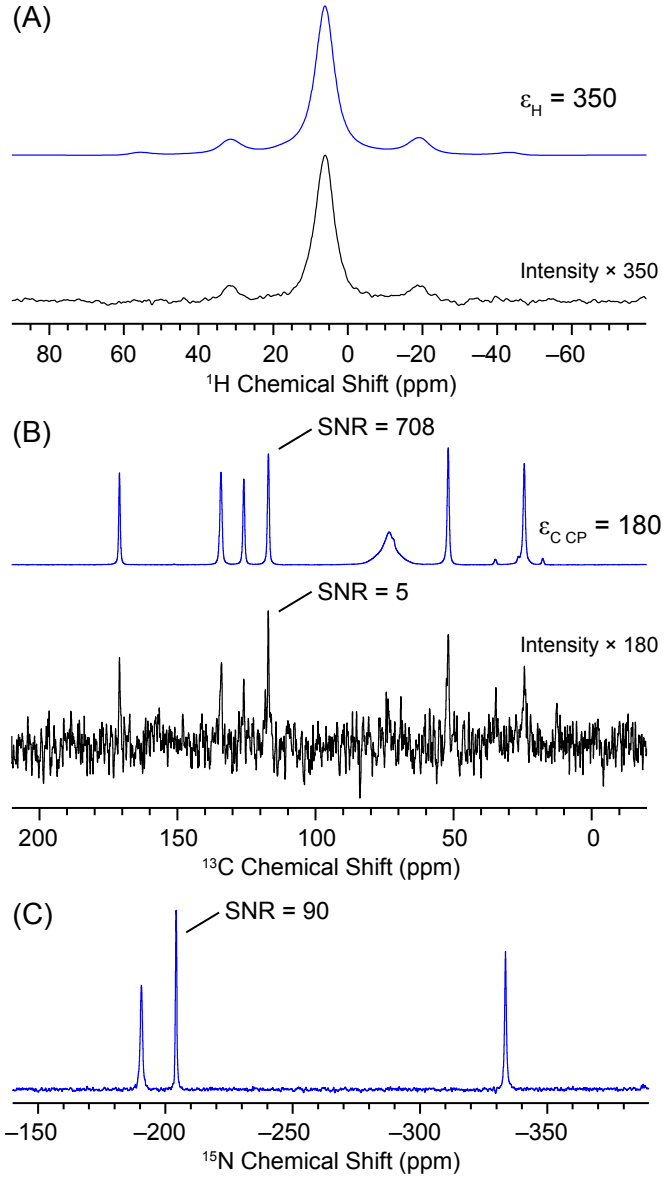

Figure 4. Examples of relayed DNP experiments on histidine•HCl•H_2O. (A) ^{1}H spin echo, (B) ^{13}C CPMAS and (C) ^{15}N CPMAS solid-state NMR spectra of finely ground histidine•HCl•H_2O impregnated with a 16 mM TEKPol TCE solution. The sample temperature was ca. 110 K. The ^{1}H and ^{13}C solid-state NMR spectra acquired with (blue traces) and without (black traces) microwave irradiation are compared to illustrate the signal enhancement provided by DNP. The signal-to-noise ratios (SNR) of the ^{13}C and ^{15}N solid-state NMR spectra are indicated. The ^{1}H, ^{13}C and ^{15}N solid-state NMR spectra were obtained with co-addition of 8 scans and a 3.0 s polarization delay, 8 scans and a 10.0 s polarization delay, and 8 scans and a 60.0 s polarization delay, respectively.

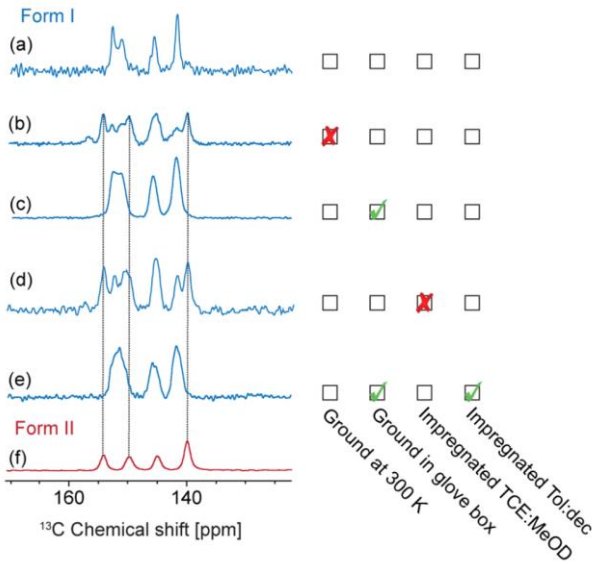

Figure 5. DNP-enhanced ^{13}C CPMAS NMR spectra recorded at 105 K of theophylline form I subjected to the different sample preparation steps associated with relayed DNP. (a) Pristine recrystallized form I theophylline. (b) Theophylline form I manually ground at room temperature, resulting in a mixture of form I and form II. (c) Form I manually ground at a temperature of ca. 220 K in a glovebox. (d) Impregnation of ground form I with a TCE/d_4-methanol TEKPol solution results in a mixture of form I and form II. (e) Ground form I impregnated with a toluene-d_8/decalin TEKPol solution shows no conversion to form II. (f) The reference spectrum of pure theophylline form II. Reprinted with permission from reference [127], Pinon, A. C.; Rossini, A. J.; Widdifield, C. M.; Gajan, D.; Emsley, L., *Mol. Pharmaceutics* **2015**, *12*, 4146. Copyright 2015 American Chemical Society.

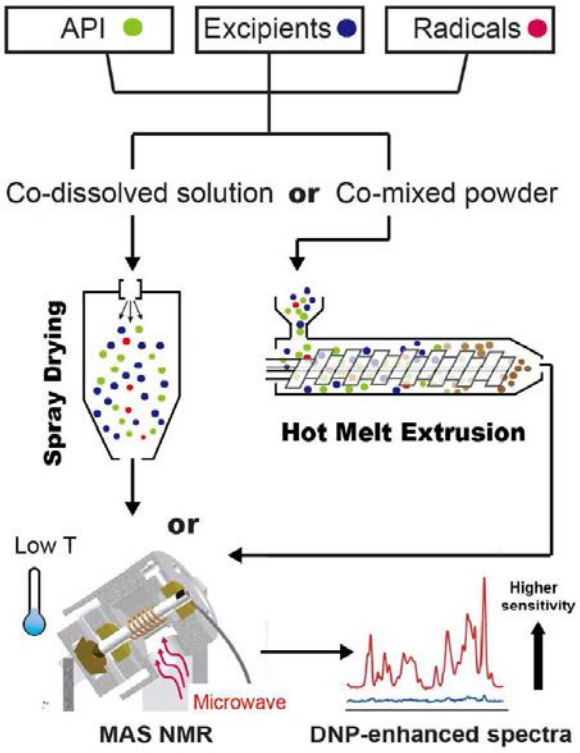

Figure 6. Illustration of the sample preparation protocols used to directly dope amorphous solid dispersions (ASDs) prepared by spray drying or hot-melt extrusion. Reprinted with permission from reference [140], Ni, Q. Z.; Yang, F.; Can, T. V.; Sergeyev, I. V.; D'Addio, S. M.; Jawla, S. K.; Li, Y.; Lipert, M. P.; Xu, W.; Williamson, R. T.; Leone, A.; Griffin, R. G.; Su, Y., *J. Phys. Chem. B* **2017**, *121*, 8132. Copyright 2017 American Chemical Society.

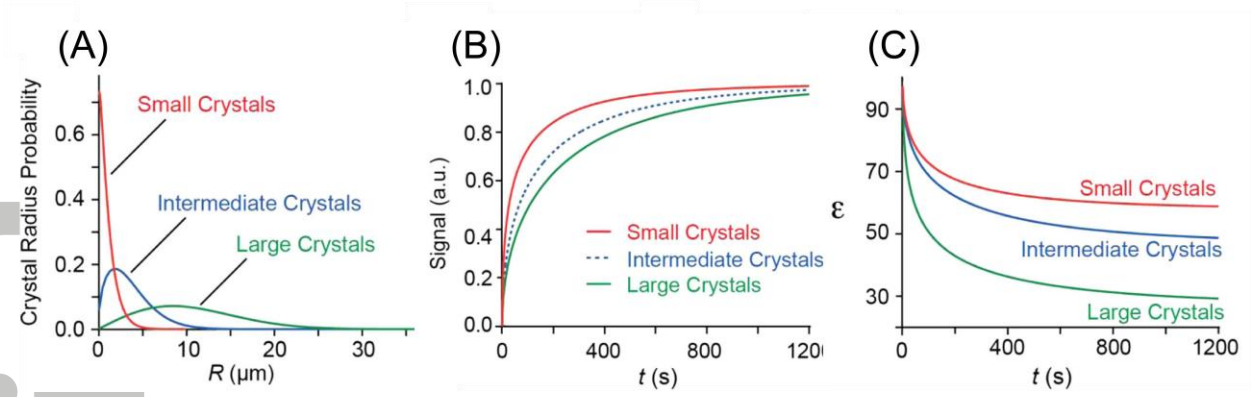

Figure 7. DNP enhancements and signal build-up rates for different spherical particle size distributions calculated by numerical solution of the diffusion equation and weighting the calculated enhancement by position, particle volume and crystal probability. (A) Different model crystal radius Weibull distributions. (B) The predicted magnitude of the signal as a function of the polarization time. (C) Predicted DNP enhancements as a function of polarization time. In all cases the proton T_1 inside the crystals was assumed to be 700 s and the DNP-enhanced proton polarization at the surface of the crystals was assumed to build-up with a time constant of 1 ms, to a polarization 100 times that of the equilibrium level (ε_0 = 100). Adapted with permission from reference [122], Rossini, A. J.; Zagdoun, A.; Hegner, F.; Schwarzwalder, M.; Gajan, D.; Coperet, C.; Lesage, A.; Emsley, L., *J. Am. Chem. Soc.* **2012**, *134*, 16899. Copyright 2012 American Chemical Society.

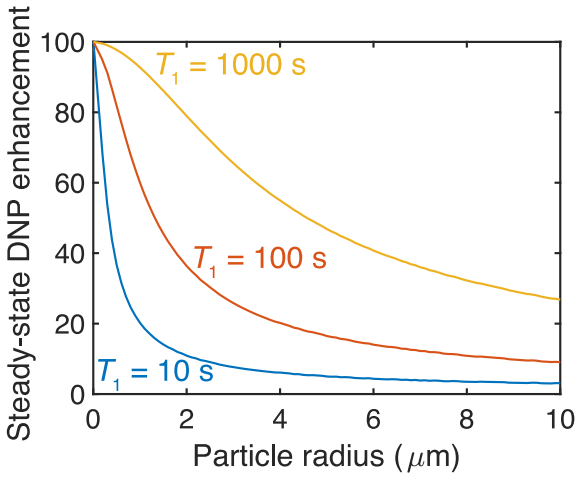

Figure 8. Simulated steady-state enhancement (ε_∞) of a spherical particle as a function of the particle radius. Curves are shown for nuclear T_1's inside the particle of 10 s, 100 s and 1000 s. In the simulation, D = 1.0 × 10^5 Å^2 s^{-1} inside of the particles and the PA solution at the surface of the particles has a build-up time of 3.0 s and ε_0 = 100.

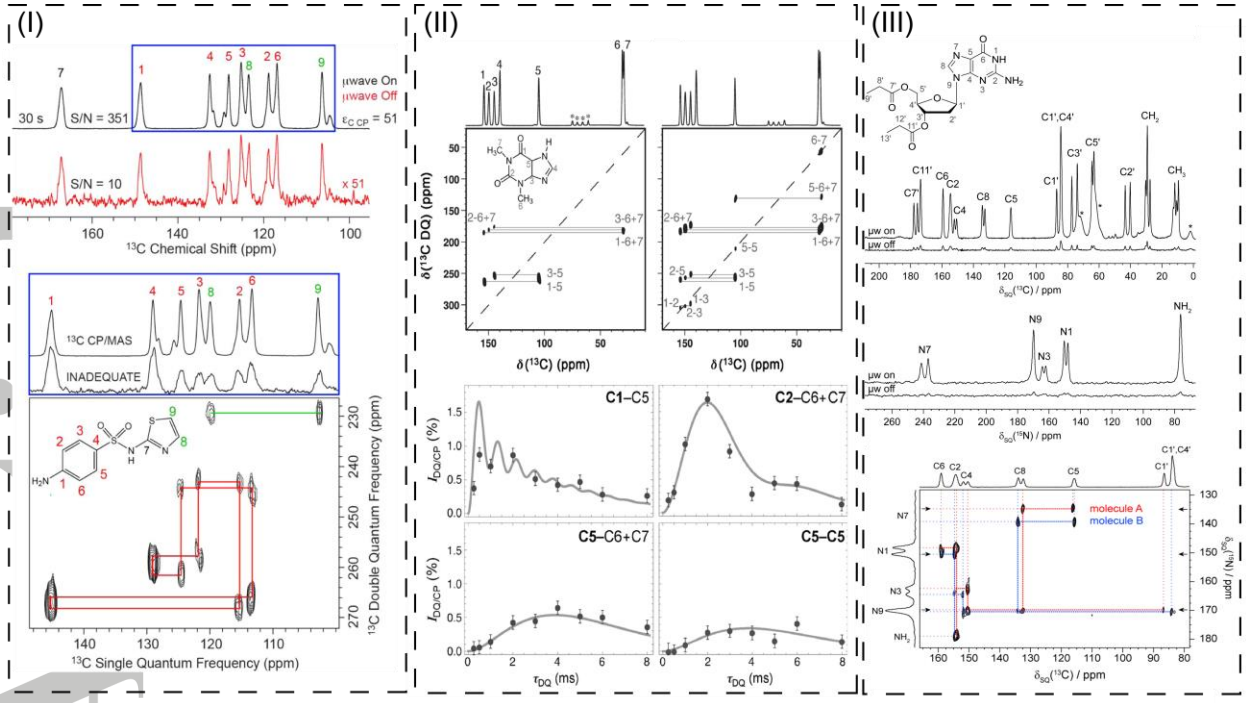

Figure 9. Examples of challenging multi-dimensional solid-state NMR experiments enabled by relayed DNP. (I) DNP-enhanced 2D scalar ^{13}C-^{13}C DQ-SQ homonuclear correlation spectrum of sulfathiazole obtained with the refocused INADEQUATE pulse sequence in a total experiment time of 16 hours. (II) DNP-enhanced 2D dipolar ^{13}C-^{13}C DQ-SQ homonuclear correlation spectra of theophylline form II and the DQ signal build-up curves extracted from 2D spectra obtained with different mixing times. The DQ signal build-up curves are fit to analytical functions corresponding to ideal build-up curves generated from the carbon-carbon distances and dipolar couplings observed in the crystal structure of theophylline. (III) DNP-enhanced 2D ^{13}C-^{15}N CP-HETCOR spectrum of a self-assembled 2′-deoxyguanosine derivative. (I) Reprinted with permission from reference [122], Rossini, A. J.; Zagdoun, A.; Hegner, F.; Schwarzwalder, M.; Gajan, D.; Coperet, C.; Lesage, A.; Emsley, L., *J. Am. Chem. Soc.* **2012**, *134*, 16899. Copyright 2012 American Chemical Society. (II) Reprinted with permission from reference [139], Mollica, G.; Dekhil, M.; Ziarelli, F.; Thureau, P.; Viel, S., *Angew. Chem., Int. Ed.* **2015**, *54*, 6028. Copyright 2015 WILEY-VCH Verlag GmbH & Co. KGaA, Weinheim. (III) Reprinted with permission from reference [176], Märker, K.; Pingret, M.; Mouesca, J.-M.; Gasparutto, D.; Hediger, S.; De Paëpe, G., *J. Am. Chem. Soc.* **2015**, *137*, 13796. Copyright 2015 American Chemical Society.

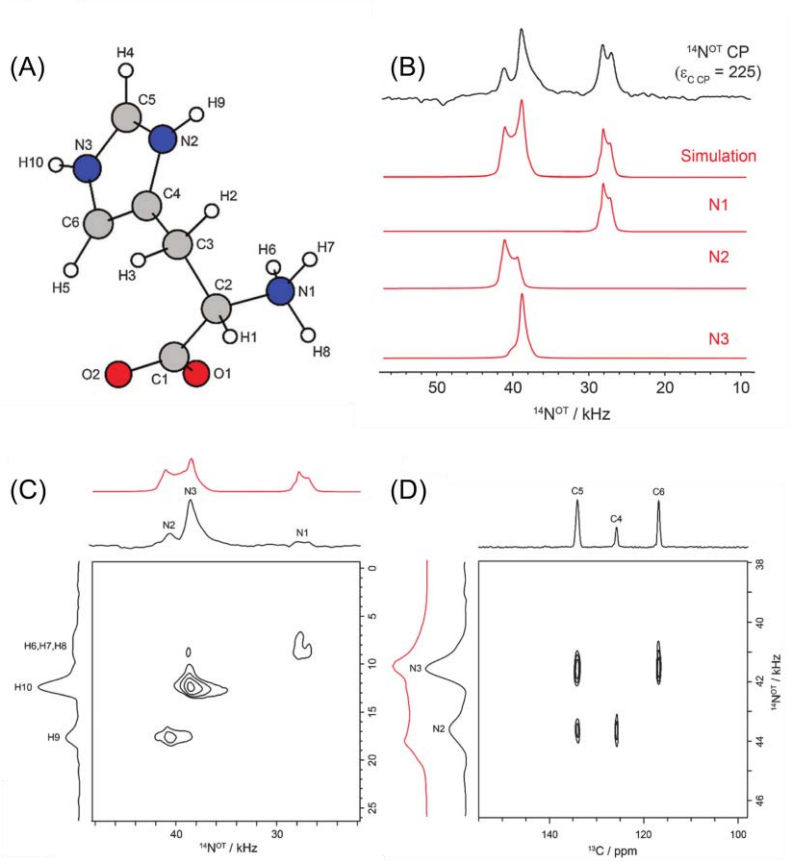

Figure 10. $^{14}N^{OT}$ solid-state NMR spectra of histidine•HCl•H_2O obtained with relayed DNP. (A) Molecular structure of histidine•HCl•H_2O and atom labeling scheme. (B) Experimental ^{1}H-$^{14}N^{OT}$ CPMAS solid-state NMR spectrum (black trace) and simulations of the $^{14}N^{OT}$ spectra of the three different nitrogen atoms. (C) 2D ^{1}H-$^{14}N^{OT}$ CP-HETCOR spectrum obtained with ^{1}H homonuclear decoupling applied during the indirect dimension evolution period. The total experiment time was approximately 8 hours. (D) 2D $^{13}C\{^{14}N^{OT}\}$ HMQC solid-state NMR spectrum. Reproduced from reference [137], Rossini, A. J.; Emsley, L.; O'Dell, L. A., *Phys. Chem. Chem. Phys.* **2014**, *16*, 12890, with permission from the PCCP Owner Societies.

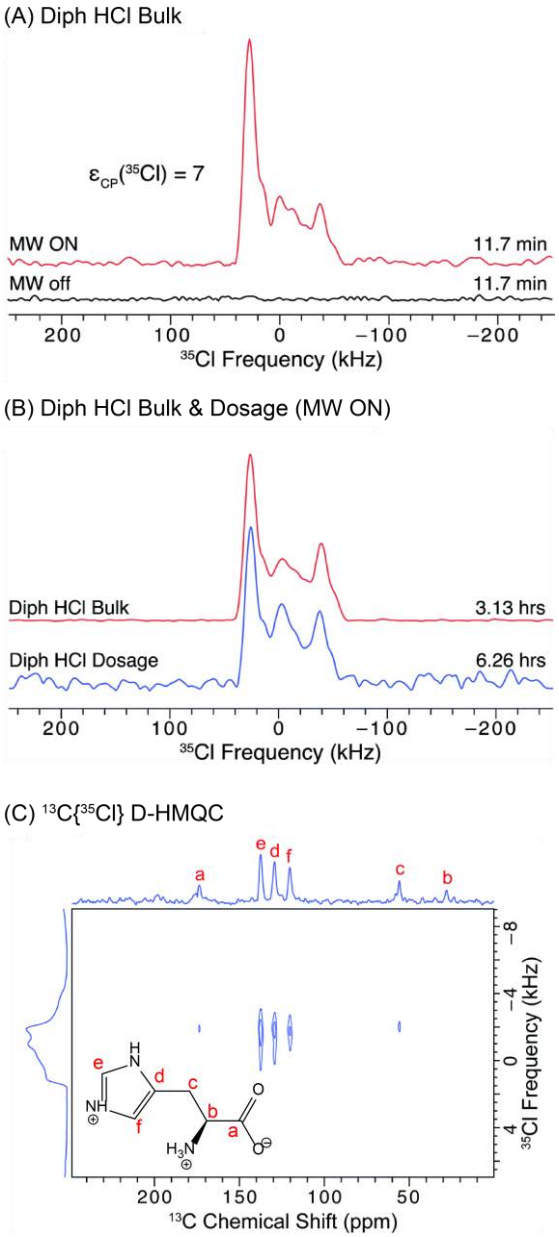

Figure 11. DNP-enhanced ^{35}Cl solid-state NMR spectra. (A) Static BRAIN-CP/WCPMG ^{35}Cl solid-state NMR spectrum of diphenhydramine HCl acquired with and without microwaves. The ^{35}Cl CP DNP enhancement was 7 and the total experiment time was 11.7 minutes. (B) Comparison of DNP-enhanced ^{35}Cl solid-state NMR spectra of bulk diphenhydramine HCl and a commercial formulation of diphenhydramine HCl which was only ca. 6 wt.% API (experiment time of 6.3 hours). (C) DNP-enhanced 2D ^{13}C{^{35}Cl} D-HMQC spectrum of histidine•HCl•H_2O obtained with rotary resonance recoupling applied to ^{13}C. The total experiment time was 14 hours. Reproduced from reference [94], Hirsh, D. A.; Rossini, A. J.; Emsley, L.; Schurko, R. W., *Phys. Chem. Chem. Phys.* **2016**, *18*, 25893, with permission from the PCCP Owner Societies.

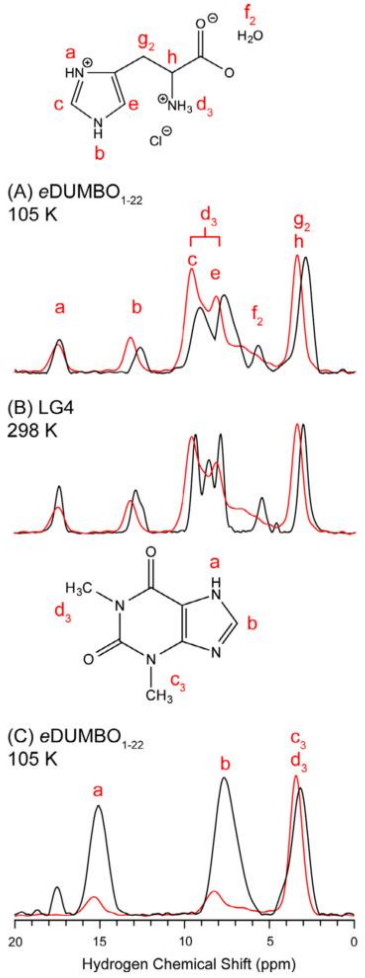

Figure 12. Comparison of DNP-enhanced natural isotopic abundance ^{2}H solid-state NMR spectra (red) and homonuclear decoupled ^{1}H solid-state NMR spectra (black) for histidine•HCl•H_2O (A and B) and theophylline (C). Reproduced from reference [138], Rossini, A. J.; Schlagnitweit, J.; Lesage, A.; Emsley, L., *J. Magn. Reson.* **2015**, *259*, 192.

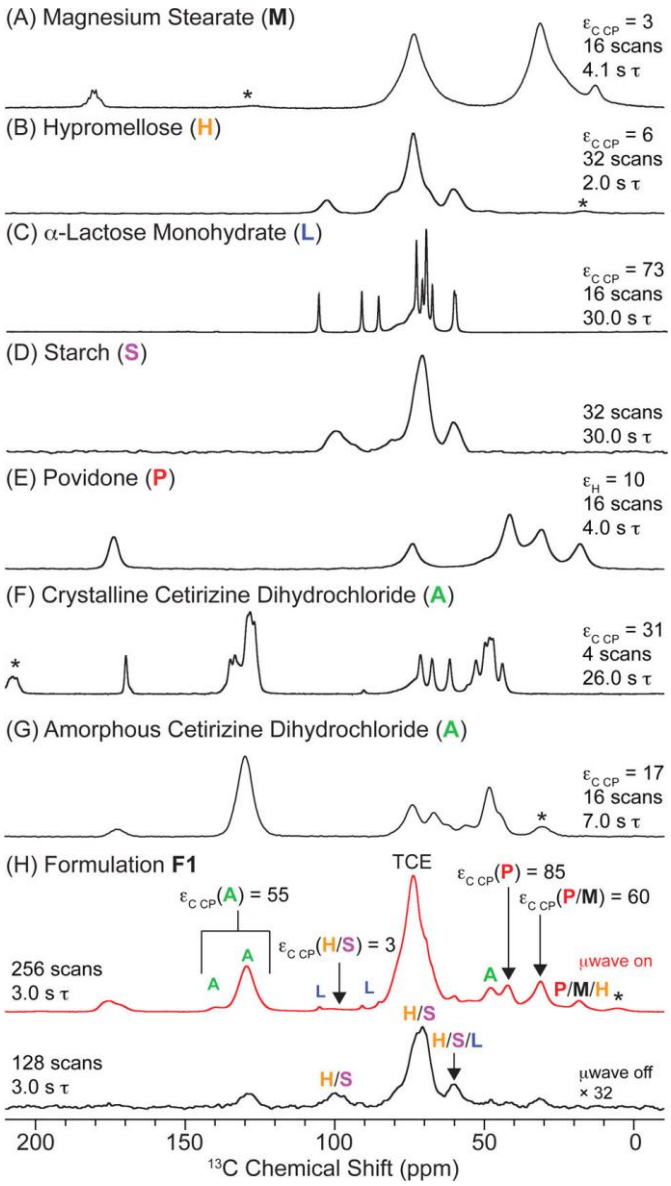

Figure 13. DNP-enhanced ^{13}C CPMAS NMR spectra of (A) magnesium stearate, (B) hypromellose, (C) α-lactose monohydrate, (D) starch, (E) povidone (F) crystalline cetirizine dihydrochloride, (G) amorphous cetirizine dihydrochloride and (H) a commercial formulation of cetirizine dihydrochloride with 8.7 wt.% API loading. DNP enhancements for each compound and the different components of the formulation are indicated. All solids were ground and impregnated with TCE solutions of TEKPol except for starch where a spectrum were acquired from the pure solid without addition of TCE. Reprinted with permission from reference [133], Rossini, A. J.; Widdifield, C. M.; Zagdoun, A.; Lelli, M.; Schwarzwalder, M.; Coperet, C.; Lesage, A.; Emsley, L., *J. Am. Chem. Soc.* **2014**, *136*, 2324. Copyright 2014 American Chemical Society.

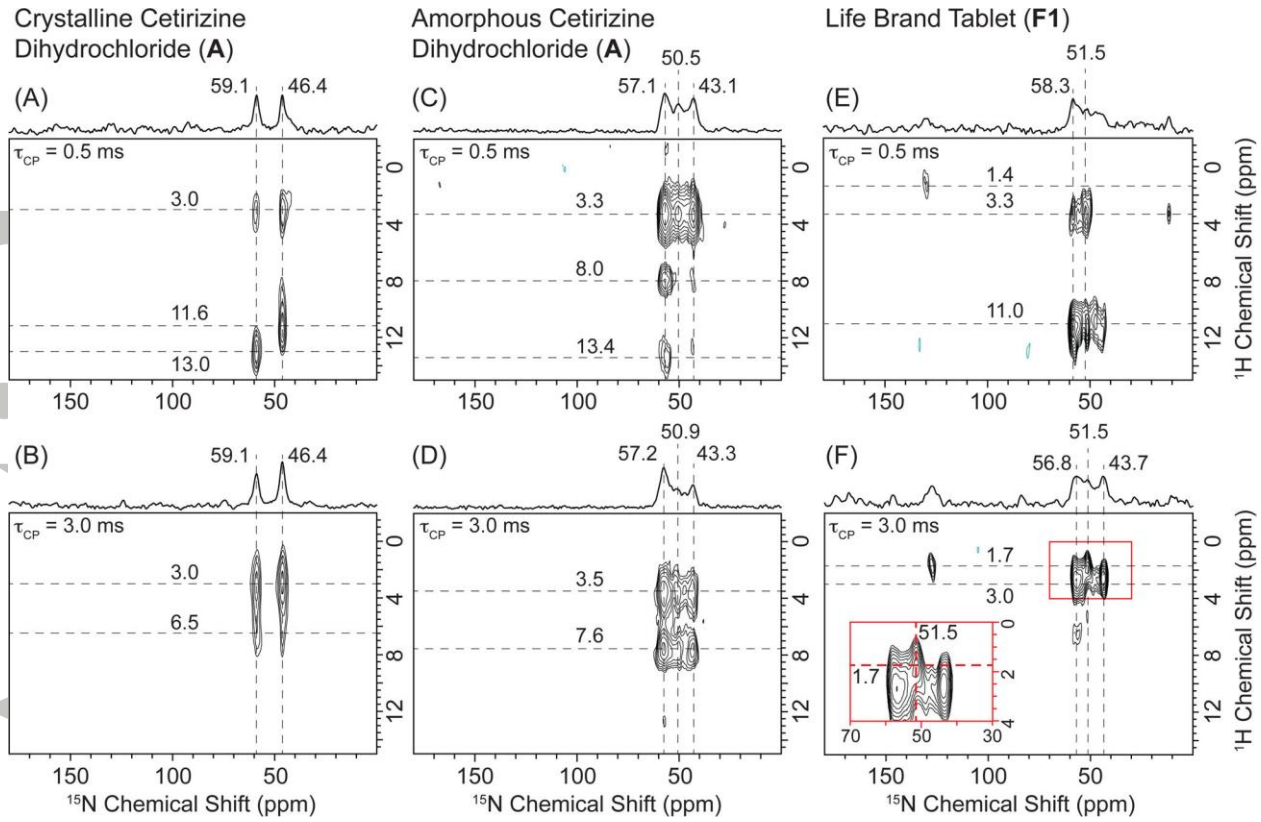

Figure 14. DNP-enhanced 2D ^{1}H-^{15}N dipolar HETCOR spectra of (A and B) crystalline cetirizine dihydrochloride, (C and D) amorphous cetirizine dihydrochloride, and an (E and F) 8.7 wt.% API tablet. The spectra were acquired with contact times (τ_{CP}) of 0.5 ms (top spectra) and 3.0 ms (lower spectra) to probe for short- and long-range ^{1}H–^{15}N distances, respectively. The total experiment times were less than 6 hours. Reprinted with permission from reference [133], Rossini, A. J.; Widdifield, C. M.; Zagdoun, A.; Lelli, M.; Schwarzwalder, M.; Coperet, C.; Lesage, A.; Emsley, L., *J. Am. Chem. Soc.* **2014**, *136*, 2324. Copyright 2014 American Chemical Society.

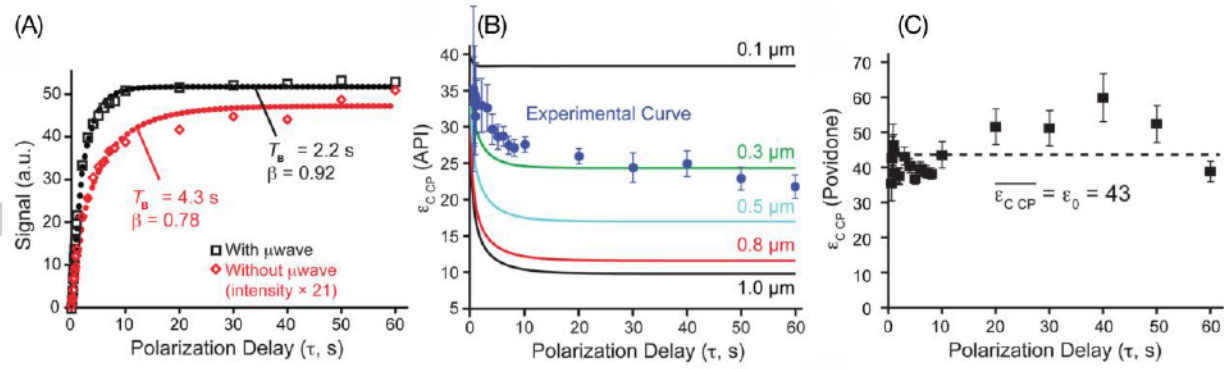

Figure 15. (A) Signal build-up observed for the API ^{13}C peak with a saturation recovery CP pulse sequenced with (black) and without (red) microwave irradiation. Filled circles are fits to stretched exponential functions of the form $S(t) = S_0\left[1 - \exp(-(t/T_B)^{\beta})\right]$. (B) Comparison between experimental and simulated $\varepsilon_{C\,CP}$ of the API as a function of the polarization delay using the numerical spherical model. Simulations are shown for different API particle radii. In the simulations, $\varepsilon_0 = 43$, $T_{1,API} = 5.3$ s, $T_{B,Source} = 2.3$ s (the T_1 at the surface of the particles) and $D = 1 \times 10^5$ Å^2 s^{-1}. (C) Experimental enhancement of the povidone ^{13}C peak as a function of time. Reprinted with permission from reference [133], Rossini, A. J.; Widdifield, C. M.; Zagdoun, A.; Lelli, M.; Schwarzwalder, M.; Coperet, C.; Lesage, A.; Emsley, L., *J. Am. Chem. Soc.* **2014**, *136*, 2324. Copyright 2014 American Chemical Society.

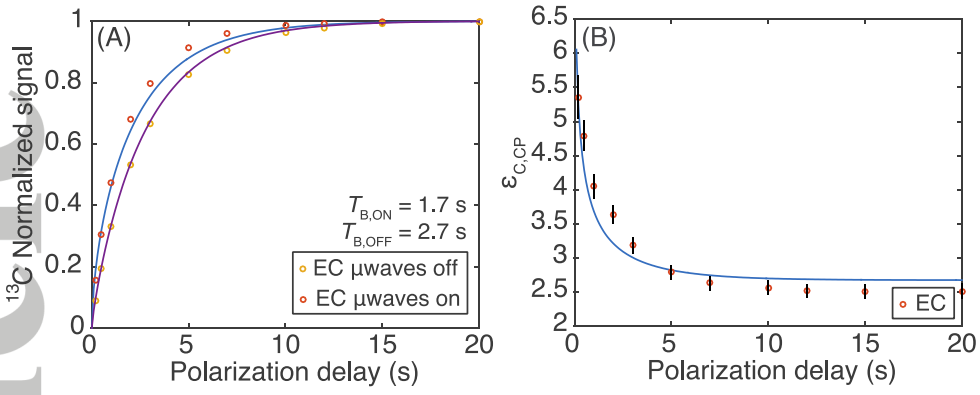

Figure 16. (A) Normalized ^{13}C CPMAS signal build-up of the EC peak in an EC/HPC film without and with microwave irradiation to drive DNP. (B) ^{13}C CP DNP enhancement of the EC peak as a function of the polarization delay. The blue line corresponds to numerical simulations of a one-dimensional diffusion model with the following parameters: L = 200 nm, $T_{B,Source}$ = 5 ms, $T_{1,EC}$ = 3.5 s, D = 2 × 10^4 Å^2 s^{-1}. Reprinted with permission from reference [155], Pinon, A. C.; Schlagnitweit, J.; Berruyer, P.; Rossini, A. J.; Lelli, M.; Socie, E.; Tang, M.; Pham, T.; Lesage, A.; Schantz, S., *The Journal of Physical Chemistry C* **2017**, *121*, 15993. Copyright 2017 American Chemical Society.

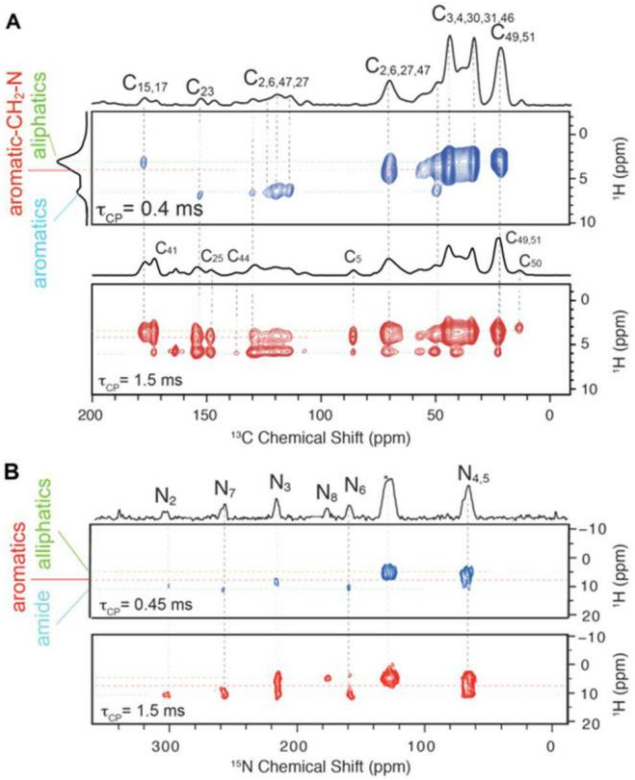

Figure 17. DNP-enhanced (A) ^{1}H-^{13}C and (B) ^{1}H-^{15}N HETCOR solid-state NMR spectra of a posaconazole-^{2}H vinyl acetate ASD directly doped with ca. 1 wt.% AMUPol. The ASD was prepared by spray drying. The 2D HETCOR solid-state NMR spectra were obtained with total experiment times of 7 hours each. Reprinted with permission from reference [140], Ni, Q. Z.; Yang, F.; Can, T. V.; Sergeyev, I. V.; D'Addio, S. M.; Jawla, S. K.; Li, Y.; Lipert, M. P.; Xu, W.; Williamson, R. T.; Leone, A.; Griffin, R. G.; Su, Y., *J. Phys. Chem. B* **2017**, *121*, 8132. Copyright 2017 American Chemical Society.

Table 1. Properties of NMR-Active Nuclei Commonly Found in APIs.[97]

Nucleus	Nuclear Spin (I)	γ (10^7 rad T^{-1} S^{-1})	Natural Isotopic Abundance (%)
^{1}H	1/2	26.8	99.99
^{2}H	1	4.1	0.015
^{13}C	1/2	6.7	1.10
^{14}N	1	1.9	99.63
^{15}N	1/2	–2.7	0.37
^{17}O	5/2	–3.6	0.04
^{19}F	1/2	25.2	100.00
^{23}Na	3/2	7.1	100.00
^{29}Si	1/2	–5.3	4.67
^{31}P	1/2	10.8	100.00
^{33}S	3/2	2.1	0.76
^{35}Cl	3/2	6.7	75.53
^{43}Ca	7/2	–1.8	0.135

Table 2. Summary of APIs and Select Organic Solids Studied by DNP-Enhanced Solid-State NMR

API/Solid	^{13}C CP DNP Enhancement ($\varepsilon_{C\ CP}$)	Polarizing Agent	Solvent/Matrix	Reference
Relayed DNP				
Acetylsalicylic Acid	7	TEKPol	1,3-DBB	[135]
Ambroxol HCl	92	TEKPol	TCE	[94]
Ambroxol HCl	54	TEKPol	OTP	[129]
Cetirizine•2HCl	20	TEKPol	1,3-DBB	[94]
Cetirizine•2HCl	31	TEKPol	TCE	[133]
Cetirizine•2HCl (Amorphous)	64	TEKPol	TCE	[133]
Dicoumarol	10	AMUPol	Glycerol-d_8:D_2O:H_2O	[135]
Diphenhydramine HCl	25	TEKPol	TCE	[94]
Furosemide	6	TEKPol	1,3-DBB	[136]
Glucose	68	bCTbK	TBE	[122]
Histidine•HCl•H_2O	225	TEKPol	TCE	[137]
Histidine•HCl•H_2O	260	TEKPol	TCE	[94]
Ibuprofen	10	TEKPol	OTP	[129]
Paracetamol	5	bCTbK	1,3-DBB	[122]
Progesterone	-[b]	AMUPol	Glycerol-d_8:D_2O:H_2O	[131]
Salicylic Acid	75	TEKPol	TCE	[135]
Sulfathiazole	51	TEKPol	1,3-DBB	[122]
Theophylline Form II	11	TEKPol	TCE	[127]
Theophylline Form I	4	TEKPol	Toluene-d_8:decalin	[127]
Theophylline Form IV	2	TEKPol	TCE	[127]
Theophylline Form M	2	AMUPol	Glycerol-d_8:D_2O:H_2O	[127]
Theophylline Form II	17	TEKPol	TCE	[138]
Theophylline Form II	12	TEKPol	$EtBr_4$	[139]
Direct-doping				
Indomethacin	14	bTtereph	-	[130]
Clotrimazole (1%, wt %)	17	AMUPol	-	[140]
Posaconazole (20%, wt %)	32	AMUPol	-	[140]
Cellulose	20	TOTAPOL	-	[141]

[a]The ^{13}C CPMAS DNP signal enhancement factor ($\varepsilon_{C\ CP}$) is determined by comparing the intensity of the NMR spectra acquired with and without with microwave irradiation and the same experimental conditions. See Figure 4 for an example. [b]The enhancement was not specified.